④

GL-TR-90-0009

AD-A221 059

MODELS OF THE EXTERNAL SOURCE CONTRIBUTION TO MAGNETOSPHERIC
MAGNETIC FIELDS FOR CRRES DATA ANALYSIS

J. N. Bass
C. E. Jordan

Radex., Inc.
Three Preston Court
Bedford, MA 01730

January 31, 1990

Scientific Report No. 2

DTIC
S
ELECTE
MAY 0 1 1990
E
D

90 04 23 036

"This technical report has been reviewed and is approved for publication"
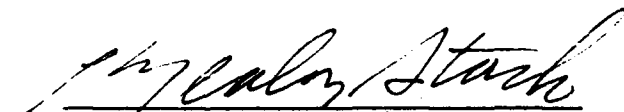
[signature]

EDWARD C. ROBINSON
Contract Manager
Data Systems Branch
Aerospace Engineering Division

[signature]

ROBERT E. McINERNEY, Chief
Data Systems Branch
Aerospace Engineering Division

FOR THE COMMANDER

[signature]

C. NEALON STARK, Director
Aerospace Engineering Division

This report has been reviewed by the ESD Public Affairs Office (PA) and is releasable to the National Technical Information Service (NTIS).

Qualified requestors may obtain additional copies from the Defense Technical Information Center. All others should apply to the National Technical Information Service.

If your address has changed, or if you wish to be removed from the mailing list, or if the addressee is no longer employed by your organization, please notify GL/IMA, Hanscom AFB, MA 01731. This will assist us in maintaining a current mailing list.

Do not return copies of this report unless contractual obligations or notices on a specific document requires that it be returned.

REPORT DOCUMENTATION PAGE

1a. REPORT SECURITY CLASSIFICATION	1b. RESTRICTIVE MARKINGS
Unclassified	

2a. SECURITY CLASSIFICATION AUTHORITY	3. DISTRIBUTION / AVAILABILITY OF REPORT
	Approved for Public Release
2b. DECLASSIFICATION / DOWNGRADING SCHEDULE	Distribution Unlimited

4. PERFORMING ORGANIZATION REPORT NUMBER(S)	5. MONITORING ORGANIZATION REPORT NUMBER(S)
RX-R-90011	GL-TR-90-0009

6a. NAME OF PERFORMING ORGANIZATION	6b. OFFICE SYMBOL (If applicable)	7a. NAME OF MONITORING ORGANIZATION
RADEX, Inc.		Geophysics Laboratory

6c. ADDRESS (City, State, and ZIP Code)	7b. ADDRESS (City, State, and ZIP Code)
Three Preston Court	Hanscom AFB
Bedford, MA 01730	Massachusetts 01731-5000

8a. NAME OF FUNDING / SPONSORING ORGANIZATION	8b. OFFICE SYMBOL (If applicable)	9. PROCUREMENT INSTRUMENT IDENTIFICATION NUMBER
		Contract F19628-89-C-0068

8c. ADDRESS (City, State, and ZIP Code)	10. SOURCE OF FUNDING NUMBERS			
	PROGRAM ELEMENT NO.	PROJECT NO.	TASK NO.	WORK UNIT ACCESSION NO
	62101F	7659	05	AB

11. TITLE (Include Security Classification)

Models of the External Source Contribution to Magnetospheric Magnetic Fields for CRRES Data Analysis

12. PERSONAL AUTHOR(S)

J. N. Bass, C. E. Jordan

13a. TYPE OF REPORT	13b. TIME COVERED	14. DATE OF REPORT (Year, Month, Day)	15. PAGE COUNT
Scientific Report #2	FROM 6/89 TO 1/90	1990, 01, 31	48

16. SUPPLEMENTARY NOTATION

17.	COSATI CODES		18. SUBJECT TERMS (Continue on reverse if necessary and identify by block number)
FIELD	GROUP	SUB-GROUP	Magnetic field, External models, ring current, tail current, Chapman-Ferraro

19. ABSTRACT (Continue on reverse if necessary and identify by block number)

The Olson-Pfitzer tilt dependent, the Mead-Fairfield, the Tsyganenko-Usmanov, the Tsyganenko 1987, the Olson-Pfitzer dynamic, and the Stern external magnetic field models are reviewed for their appropriateness for use in analysis of data from the Combined Release and Radiation Effects Satellite (CRRES). Descriptions of the models and their derivations are given. The Stern model requires considerably more computation time than the others. The L-parameter computed with an internal plus external field deviates considerably from that obtained with the internal field alone at the larger radial distances in CRRES's range. The models also differ noticeably from one another. The magnetic field magnitudes computed from the models during a SCATHA orbit over a magnetically quiet period agree well with SCATHA magnetometer observations. The Olson-Pfitzer dynamic model best tracks the data. However during the subsequent orbit, none of the models depict the large observed substorm-associated depression. The equatorial midnight field depression predicted by the Olson-Pfitzer dynamic model at zero dipole tilt is larger at small distances than that implied by averaged AMPTE and OGO measurements; the Stern and Olson-Pfitzer tilt dependent models are in good agreement with the measurements, while the other models predict smaller depressions. It is concluded that the Olson-Pfitzer dynamic model is the best to use for CRRES, primarily because of its parameterization and its superior data base in the CRRES range.

20. DISTRIBUTION / AVAILABILITY OF ABSTRACT	21. ABSTRACT SECURITY CLASSIFICATION
☒ UNCLASSIFIED/UNLIMITED ☐ SAME AS RPT. ☐ DTIC USERS	Unclassified

22a. NAME OF RESPONSIBLE INDIVIDUAL	22b. TELEPHONE (Include Area Code)	22c. OFFICE SYMBOL
E. C. Robinson	(617)377-3840	GL/LCY

DD FORM 1473, 84 MAR — 83 APR edition may be used until exhausted
All other editions are obsolete

ACKNOWLEDGEMENTS

DTIC COPY INSPECTED

TABLE OF CONTENTS

LIST OF FIGURES

LIST OF TABLES

vi

1. INTRODUCTION

In the earth's magnetosphere the magnetic field is the sum of two parts: that which we will call the "internal" field, because it is due to sources (currents) in the earth's interior, and that which we will call the "external" magnetic field, because it is due to sources outside the earth's surface. Because its sources are in the interior of the earth, the internal field at a point outside the earth's surface is curl-free:

$$\nabla \times B_{int} = 4\pi J/c = 0 \tag{1}$$

Here B_{int} is the internal magnetic field vector, J is the current density, and the equation is in cgs units. Therefore B_{int} can be expressed as the gradient of a scalar potential:

$$B_{int} = -\nabla V \tag{2}$$

Here the negative sign is used, consistent with the mechanical relationship between potential energy and force, although some authors use the positive sign. Since B_{int} is also divergence-free, the scalar potential satisfies Laplace's equation:

$$\nabla^2 V = \nabla \bullet (\nabla V) = -\nabla \bullet (B_{int}) = 0 \tag{3}$$

Therefore V may be expanded in spherical harmonics:

$$V = a \Sigma_{nm} (a/r)^{n+1} P_n^m(\cos\lambda)(g_n^m \cos m\phi + h_n^m \sin m\phi) \tag{4}$$

where r, λ, and ϕ are the radial distance, geographic colatitude, and east longitude, a is the earth's radius, P_n^m are associated Legendre functions, and g_n^m and h_n^m are the coefficients. Internal field models may thus be defined using equations (2) and (4) [*Jordan and Bass*, 1989]. No attempt has been made to specify explicitly the relevant current sources.

The principal feature distinguishing the external field from the internal field is the location of the source. A point outside the earth's surface may be embedded within currents contributing to the external field. Thus the external field, unlike the internal, is not, in general, current-free, and usually cannot be expressed as the gradient of a scalar potential. However, since the external currents are more amenable to observation, more can be said about them than the internal currents. Thus external field modeling has frequently begun with models of the current, from which the field is subsequently derived. The currents included in most models are those known as ring currents, cross-tail currents, and magnetopause currents. The ring currents, carried by trapped ions and electrons in the 20-50 keV energy range, circulate longitudinally around the earth at distances 2-7 R_E. The cross-tail currents flow from dawn to dusk across the night-side plasma sheet. Some models also include the associated return currents, flowing around the magnetopause from dusk to dawn. The magnetopause currents are the Chapman-Ferraro boundary currents, which are formed by the interaction of the magnetosphere with the solar wind. The field due to the magnetopause currents alone can be expressed in terms of a scalar potential (for points inside the magnetosphere). Primary examples, discussed below, of models which include magnetopause currents are the models of Mead [1964] and Stern [1985]. There is another system of currents, the field-aligned currents, which none of the models to be discussed here include explicitly.

The CRRES satellite will provide data for a generation of new models of the earth's radiation belts. Because the orbits of the trapped high energy radiation belt particles are controlled by the earth's magnetic field, the accuracy of the models will largely be determined by the accuracy of the magnetic field models used in ordering the data. Present radiation belt models neglect the external magnetic field. While this approximation may be acceptable for the inner belt, it becomes questionable at larger distances, as the external field accounts for an increasing fraction of the total field.

This report reviews the models listed in Table 1. Section 2 discusses the derivation and mathematical construction of these models. Section 3 discusses a software system we have developed for the studies of properties of these models, including routines to compute the models themselves. A comparison of computation times for the models is given.

Table 1. External Magnetic Field Models

Olson-Pfitzer Tilt Dependent [*Olson and Pfitzer*, 1977]
Olson-Pfitzer Dynamic [*Pfitzer, et. al.*, 1988]
Mead-Fairfield [*Mead and Fairfield*, 1975]
Tsyganenko-Usmanov [*Tsyganenko and Usmanov*, 1982]
Tsyganenko [*Tsyganenko*, 1987]
Stern Parabolic Magnetopause/Stretched Magnetosphere [*Stern*, 1985, 1987]

Of primary interest for radiation belt analysis are the properties of the McIlwain L parameter and the magnitude of the total (internal + external) magnetic field vector, since these have been the traditional sorting parameters for modeling the trapped particle populations. In section 4, comparisons of the L parameter among the models are presented. In section 5, we compare the total magnetic field vector derived from the models with those observed by the SCATHA satellite for a quiet and a moderately active period. Also in section 5, model depiction of the night side equatorial magnetic field depression as a function of distance is compared with averaged measurements by the AMPTE and OGO satellites. The equatorial field is critical to the magnetic mapping of auroral phenomena to the plasma sheet.

We conclude in Section 6 that of the models studied, the Olson-Pfitzer dynamic model is currently the best to use for CRRES for the following reasons: a) its inputs are parameters relating to specific magnetospheric processes, and these can be adjusted in real time based on observations; b) its data base provides the best overall coverage in the region of interest to CRRES. However, the Olsen-Pfitzer dynamic model has shortcomings, principally, that it is valid only for zero tilt, and it is not rigorously divergence-free.

2. MODEL DERIVATION AND DESCRIPTION

Most of the models begin with some description of the three current systems we mentioned above: the ring currents, the cross-tail currents, and the magnetopause currents. The contributions of these three current systems are modeled separately and summed to produce the total magnetic field vector. A singular exception to this rule is the modified Mead model [*Bass et al.*, 1989], which, following the original Mead [1964] formulation is expressed as the negative gradient of the scalar potential:

$$V_{ext} = -B_1 \, r \cos\theta + B_2 \, r^2 \sin\theta\cos\theta\cos(t-\phi) \tag{5}$$

where r is the radial distance, θ is the geomagnetic colatitude, t is the geomagnetic local time (midnight=0°), and B_1, B_2, and ϕ are adjustable parameters. For the magnetically quiet 20 April, 1979, the SCATHA magnetometer data fit well to this model for:

$$B_1 = -10 \text{ nT}$$

$$B_2 = 2.5 \text{ nT}$$

$$\phi = -3 \text{ hours}$$

Mead's model only attempted to include the magnetopause contribution, which is curl-free and can therefore be represented as the gradient of a scalar potential. The adjustment of parameters to fit a real data situation is possibly valid for a magnetically quiet day such as this, at points inside the inner edge of the plasma sheet, because the ring current is weak, and the cross-tail currents lie in the plasma sheet and beyond.

In this report we will frequently refer to the Solar Magnetic (SM) and Geocentric Solar Magnetospheric (GSM) coordinate systems, following the terminology of Russell [1971]. In both systems the x-z plane contains the dipole and the Earth-Sun line, while the y axis is positive toward dusk. In the SM system the z axis is parallel to the dipole, positive toward the north, while the x axis is positive on the sunward side of the dipole. In the GSM system, the x axis is along the Earth-Sun line, positive toward the Sun, while the z axis is positive on the northward side of the Earth-Sun line.

2.1 OLSON-PFITZER TILT DEPENDENT MODEL

The Olson-Pfitzer tilt dependent model [*Olson and Pfitzer*, 1977] is a revision of the tilt-averaged model of Olson and Pfitzer [1974]. Tilt here refers to the complement of the Sun-dipole angle. The motivation for the revision was that the tilt-averaged model is not a good representation of the zero tilt case, primarily at large distances on the midnight equator. When the dipole is tilted, the plasma sheet has been observed to be parallel with the GSM equatorial (x-y) plane, but not coincident with it [*Stern*, 1976]. Simple models [*Murayama*, 1966; *Speiser and Ness*, 1967; *Fairfield and Ness*, 1970] postulate that the plasma sheet is hinged to the dipole equatorial plane 8-11 R_E from the Earth. Locations on the dipole equator outside the hinging distance are therefore in the plasma sheet only when the dipole is untilted. Since the plasma sheet is an area of minimum field strength, the field at zero tilt is generally smaller than the average field for such points on the dipole equator.

The SM components of $\mathbf{B}_{ext}$ are expressed as sums of terms of the form

$$[A_{ijk} + B_{ijk} \exp(-0.06r^2)]x^i y^j z^k$$

where the coefficients A_{ijk} and B_{ijk} are simple linear or quadratic functions of the tilt. The model contains no dependence on magnetic activity, but is proposed as an average model for quiet conditions ($K_p = 0, 1$). Spatially it is valid from 2.5 R_E to 15 R_E, except beyond the noon magnetopause at 10.5 R_E.

2.1.1 Model Derivation

Like the 1974 tilt-averaged model, the tilt-dependent model was constructed by first considering models for the current systems. The magnetopause currents are similar to those developed by Olson [1969] from a self-consistent solution to the Mead-Beard pressure balance condition. However, for the tilt-dependent model, an empirical shape for the magnetopause surface was chosen, instead of Olson's self-consistent solution. Magnetopause currents and their resulting contribution to the field were computed numerically.

The ring and cross-tail currents are constructed from a system of wires [Olson, 1974]. The ring currents were made from appropriately placed elliptical wires, such that their noon crossings were at lower radial distances than their midnight crossings. Therefore the resulting ring current is not azimuthally symmetric; however, dawn-dusk symmetry was retained by placing the elliptical foci on the SM x axis. The flow in the inner three wires is eastward, while in the remaining wires, it is westward. The boundary between eastward and westward current density is ~5 R_E at midnight, 3 R_E at noon. The cross-tail currents are constructed from loops consisting of dawn-to-dusk flow on the northern and southern surfaces of the hinged plasma sheet (Δz_{GSM} = ±3 R_E), coupled, respectively, to return currents over the northern and southern surfaces of the magnetopause. The loops are tilted relative to the normal to the plasma sheet in order to model the decay of B_z with increasing distance down the tail. When the dipole is tilted, the loops near the inner edge are tilted toward the normal to the dipole equator plane.

Parameters specifying the wires (position, orientation, size, and shape), their currents, and the magnetopause shape were adjusted so that the resulting total external field fit OGO-3 and -5 observations in the inner magnetosphere [Suqiura, et. al., 1971], and Explorer-33 and-35 observations in the tail [Mihalov, et. al., 1968; Behannon, 1970; Meng and Mihalov, 1972]. The resulting field, still numerical in form, was then fit by linear least squares to the analytic series described above.

2.2 OLSON-PFITZER DYNAMIC MODEL

This model [Pfitzer, et. al., 1988] is the result of a series of event studies performed for NASA Coordinated Data Analysis Workshops (CDAW). The principal feature of this model is the introduction of variable strength factors multiplying the quiet models of the fields of the three current systems. The magnetopause strength factor varies inversely as the cube of the standoff distance, which may be computed from the solar wind pressure and speed by:

$$R_{st} = 98/(nv^2)^{1/6} \tag{6}$$

4

with R_{st} in R_E, n the solar wind ion density in particles/cc, and v the solar wind speed in km/sec. The quiet model assumes R_{st} = 10.5 R_E. The field due to the magnetopause is scaled geometrically in accordance to this scaling of the magnetopause. Thus, the field at the position r due to the scaled magnetopause is

$$B(r,R_{st}) = k^{-3} B_{quiet}(r/k) \tag{7}$$

where $k = R_{st}/10.5$

This scaling is explored in more detail in Section 2.5.1. The contribution due to the tail current system is scaled in the same way as the magnetopause contribution, both in strength and geometry. There is no apparent justification for this, except that a suitable alternative has not been found [*Pfitzer*, 1989]. An index suggested by Akosofu [*Olson and Pfitzer*, 1982] which was successfully employed in tail field modeling for the CDAW 2 event, was found to be unsatisfactory for subsequent events. The ring current system is scaled in strength only, using the DST index:

$$S_{ring} = 1.0 - 0.03 \ DST \tag{8}$$

The unscaled (quiet) models of these syste as are similar in mathematical form to the quiet tilt-dependent model. However, the dynamic model is valid only for zero tilt. Spatially the model is valid from 2.5 R_E to 60 R_E on the night side, and out to the magnetopause on the day side.

2.3 MEAD-FAIRFIELD MODEL

In the Mead-Fairfield model [*Mead and Fairfield*, 1975] each component of **B** is expressed as an expansion in products of polynomials in the SM coordinates and the dipole tilt. The SM coordinates are actually rotated westward by the approximate solar wind aberration angle of 4° (the shift in the solar wind direction due to the orbiting Earth). Thus there is symmetry about a plane 4° west of the noon-midnight meridian, rather than about the noon-midnight meridian itself. For each of 4 K_p bins (0,0$^+$; 0-2 ; 2-9; 3-9) the coefficients were derived from the data by least squares, enforcing the zero divergence condition by a set of linear constraints on the coefficients. The model provides no description of the individual current systems, but the total current can be derived by taking the curl of the magnetic field vector.

The data base consisted of 12,616 averaged vector measurements by magnetometers on board satellites Explorer 33 (IMP A-D), Explorer 34 (IMP 4), Explorer 41 (IMP 5), and Explorer 43 (IMP 6) [*Behannon*,1968; *Fairfield*, 1969; *Fairfield and Ness*, 1972; *Fairfield*, 1974]. The averaging was over half-earth radii, which typically spanned 10-15 minutes. The data base contains gaps in the near-Earth equatorial region, and at high southern latitudes. Specifically there are few measurements within 5 R_E of the Earth, and none within 4 R_E. Thus the model is valid for radial distances between 5 and 15 R_E.

2.4 TSYGANENKO-USMANOV AND TSYGANENKO MODELS

The Tsyganenko-Usmanov [*Tsyganenko and Usmanov*, 1982] and Tsyganenko [1987] models are expressed as sums of the contributions from the three external sources mentioned above. The ring current and tail current contributions are expressed analytically by functions which are the curls of vector potentials; hence their divergences vanish identically. Both models employ a mathematically simple azimuthally symmetric ring current circulating around the dipole. In contrast to the Olson-Pfitzer models, the ring current flow direction is westward, independent of distance from the Earth. Accurate modeling of the innermost region was not attempted due to insufficient data coverage (see Section 2.4.4). In the Tsyganenko-Usmanov model, the tail current flows mainly from dawn to dusk on a flat sheet "hinged" or offset a distance z_0 on the GSM z-axis due to the dipole tilt. In the Tsyganenko 1987 model, this is complemented by flat current sheets at $Z_{GSM} = \pm 30\ R_E$ to simulate the return currents. Each sheet is parallel to the central sheet with minus half the current. Both models use tilt-dependent products of polynomials and decaying exponentials in the coordinates to represent the magnetopause current contribution. For these, the zero divergence condition was enforced while determining the coefficients. The data bases for these models contain the Mead-Fairfield data base as a subset. The Tsyganenko data base is more extensive at large distances down the tail; hence it has a more elaborate tail model.

2.4.1 Ring Current Model

The ring current field in both models is given by:

$$B\rho = B_0[12\rho'z'/(\rho'^2 + z'^2 + 4)^{5/2}] \tag{9a}$$

$$B_z = 4B_0[(2z'^2 - \rho'^2 + 8)/(\rho'^2 + z'^2 + 4)^{5/2}] \tag{9b}$$

$$B\phi = 0 \tag{9c}$$

Where $\rho' = \rho/\rho_0$, $z' = z/\rho_0$, ρ, z, and ϕ are cylindrical coordinates with the z axis parallel to the dipole, and B_0 and ρ_0 are adjustable parameters. The maximum ring current density is located at $\rho = \rho_0$, while the strength of the current is proportional to B_0.

2.4.2 Tail Current Models

The Tsyganenko-Usmanov tail model may be described by first considering a flat sheet of current filaments aligned in the dawn-dusk (y) direction. The sheet, of width S, has a near-Earth boundary at $x_{GSM} = x_N$, a down-tail boundary at $x_{GSM} = x_N - S$, and infinite extension in both dawn and dusk directions. Furthermore, the filaments have a finite half-thickness scale parameter D, such that the field due to any one of them is proportional to

$$(R/D)/(1 + R^2/D^2)$$

where R is the distance from the the central axis of the filament. The current distribution along the tail is

$$I(x) = (c/2\pi)[B_N + \Delta B(x - x_N)/S] \tag{10}$$

where c is the speed of light, and B_N and ΔB indicate, respectively, the current at the near-Earth boundary of this distribution and the decrease in current from this boundary to the down-tail boundary.

6

Then the contributions to the field due to a filament at x_0 are

$$dB_x = z [(x-x_0)^2 + z^2 + D^2]^{-1} [2I(x_0)/c]dx_0 \qquad (11a)$$

$$dB_y = 0 \qquad (11b)$$

$$dB_z = -(x-x_0) [(x-x_0)^2 + z^2 + D^2]^{-1} [2I(x_0)/c]dx_0 \qquad (11c)$$

Though these can be integrated analytically, the results will not be repeated here.

The field due to a sheet of infinite extension in the dawn-dusk direction was found to produce discrepancies between the model and observations in the dawn and dusk regions of the near magnetotail. Thus the model field described above has been modified by multiplication by the factor

$$f(y) = [1 + (y/\Delta y)^2]^{-1} \qquad (12)$$

This does not alter the zero divergence of **B**. The currents which produce this modified field are no longer straight. On the equator the currents make a gradual transition from straight lines in the far tail to curved lines, resembling the ring currents, in the near tail.

As mentioned previously, the tail sheet does not remain on the dipole (SM) equator when the dipole is tilted. Rather it remains parallel to the original untilted dipole (GSM) equatorial plane, and attached to the tilted dipole equator at the characteristic hinging distance. The z coordinate of a point is given by

$$z = z_{GSM} - r_H \sin \psi \qquad (13)$$

where r_H is the hinging distance, ψ is the tilt, and $r_H \sin \psi$ is equal to the distance of the tail sheet from the GSM equator.

In summary, the Tsyanenko-Usmanov tail model is described by 7 physically meaningful parameters:

the current per unit length at the near-Earth boundary of the current distribution (B_N);
the decrease in the current per unit length between the near-Earth and down-tail boundaries of the sheet (ΔB);
the location of the near-Earth boundary of the current sheet (x_N);
the distance between the near-Earth and down-tail boundaries (S);
the thickness of the filaments (D);
the scale distance in the dawn-dusk direction (Δy);
the hinging distance (r_H)

The Tsyaganko model tail field is similar, but with a more complex current distribution:

$$I(x) = (c/2\pi)[B_0 + B_1/(x-x_1) + B_2/(x-x_2)^2] \qquad (14)$$

Furthermore, one sheet has been added both 30 R_E above and below the GSM equator, with current equal in magnitude to half the central sheet current, and flowing in the opposite direction, to simulate return currents. This addition also removes the need for a finite extension of the sheets in the tailward direction; the mathematical divergences encountered by use of just

7

the single sheet are canceled by the two return current sheets. Hence in the Tsyganenko model the sheets extend infinitely in the tailward direction.

2.4.3 Magnetopause Current Models

The magnetopause current expansion consists of products of powers of the coordinates y and z perpendicular to the Earth-Sun line, decaying exponentials down tail, and the sine and cosine of the tilt angle. There is no explicit physical connection of the parameters with any current structure; thus the zero divergence criterion is not automatically satisfied for any set of chosen parameter values. The divergence requirement was therefore imposed by a set of linear constraints on the parameters during the least squares fitting procedure. There are 16 linear coefficients in the Tsyganenko-Usmanov magnetopause model, and a single nonlinear parameter specifying the exponential decay down the tail. The Tsyganenko model contains 22 linear parameters and two nonlinear parameters. The authors assert that these terms also include average contributions of field aligned currents.

2.4.4 Model Derivation

The Tsyganenko-Usmanov data base consists of the Mead-Fairfield data set and data from the HEOS-1 and HEOS-2 spacecraft [*Hedgecock and Thomas*, 1975]. The additional data are 6248 vector averages in the radial range 6-35 R_E. In the Tsyganenko data base this is augmented by 11,150 similar averages from six IMP spacecraft (A, C, E, F, G, and I) in the range -66 $R_E \leq$ $x_{GSM} \leq$ -15 R_E, and 6675 averages from IMP-H and IMP-J at down-tail distances 25-45 R_E. This additional down tail data apparently motivated the refined Tsyganenko tail model. Of particular note is that the additional data (in both models) do not fill in the near-Earth gap left by the Mead-Fairfield model data base. Therefore these two models must also be suspect within 5 R_E of the Earth. The minimal coverage of the Tsyganenko-Usmanov data set beyond 20 R_E down tail defines the limit for that model. The Tsyganenko model is supplied in two versions - a long version valid to 70 R_E, and a short version valid to 30 R_E.

As for the Mead-Fairfield model, the data were sorted into K_p bins (11 in the Tsyganenko-Usmanov model, 6 in the Tsyganenko long version, and 8 in the Tsyganenko short version). An iterative least squares method was employed because of the nonlinear parameters. In each iteration, the linear parameters were computed by standard linear least squares, freezing the nonlinear parameters at their current values. Then the nonlinear parameters were adjusted by a search method to reduce the sum of the squared residuals. Generally 4 iterations were sufficient. In the Tsyganenko-Usmanov model the ring current scale radius ρ_0 and the tail current sheet width S were held fixed. The authors attributed difficulty in determining ρ_0 to the lack of near-Earth data. However this parameter was varied in the later Tsyganenko model. The finite tail current width was an artificial device introduced to suppress mathematical divergences in the Tsyganenko-Usmanov model. Its need was eliminated by the introduction of the return tail current sheets in the Tsyganenko model. In the short Tsyganenko model, the third term in the tail current distribution has been dropped, and the magnetopause current expansion has been shortened.

8

2.5 STERN PARABOLIC MAGNETOPAUSE - STRETCHED MAGNETOSPHERE MODEL

The field due to the magnetopause currents is represented within this boundary as the gradient of a scalar potential satisfying Laplace's equation [*Stern*, 1985]. The requirement of a closed magnetosphere, i. e., that the field lines of the total field do not cross this boundary, leads to the condition that the normal component of the boundary field must cancel the normal component of the total field due to internal sources (dipole, ring current, etc.). Since the boundary is assumed to be parabolic, the solution can be expanded in parabolic harmonics, analogous to the use of spherical harmonics for problems with spherical boundaries. The axis of the boundary is the GSM axis, and its nose is at local noon. No attempt is made at a self-consistent solution of the pressure balance condition. Thus there is no dependence of the shape on the dipole tilt.

The use of a continuous boundary shape contrasts with Voigt's [*Voigt*, 1973] use of a cylinder on the night side capped by a hemisphere on the day side. Voigt's solution requires two expansions: one in cylindrical harmonics, and the other in spherical harmonics, which must be joined at the connection between the day side hemisphere and the night side cylinder. Thus Stern's approach is simpler, although perhaps less accurate at large distances down the tail, where the actual boundary shape is more like Voigt's.

The ring current field is modeled with the Tsyganenko-Usmanov expression. The total field due to the dipole and cross-tail currents is simulated by a stretched magnetosphere model [*Stern*, 1987]: the field at any point is represented in terms of the dipole field at some other location, specified by a stretching function. Both the stretched dipole and ring current fields are accounted for in the boundary conditions. The solution for the pure dipole has a simple scaling property with respect to pure linear scaling of the boundary. The ring current solution has a similar property, if the dimension of the ring current is also scaled.

2.5.1 Magnetopause Field

The magnetopause field is represented as the negative gradient of a scalar potential expressed as an expansion in parabolic harmonics (Fourier-Bessel expansion):

$$V = \Sigma_{mn} \, (a_{mn} \sin m\phi + b_{mn} \cos m\phi) \, J_m(k_{mn}\mu)I_m(k_{mn}\lambda) \qquad (15)$$

where

$$\lambda = [r+x]^{1/2}$$

$$\mu = [r-x]^{1/2}$$

$$\sin \phi = z/[x^2 + y^2]^{1/2}$$

$$\cos \phi = y/[x^2 + y^2]^{1/2}$$

$$x = x_{GSM} - x_0$$

$$y = y_{GSM}$$

$$z = z_{GSM}$$

$$r = [x^2 + y^2 + z^2]^{1/2}$$

9

x_0 = displacement, along the x_{GSM} axis, of the
focal point of the constant λ and μ surfaces

J_m = Bessel function of the first kind

I_m = Modified Bessel function of the first kind

k_{mn} = roots of $J_m(k_{mn}A) = 0$

A = the desired range of the expansion in μ

In the parabolic coordinate system, the constant λ surfaces are paraboloids of revolution about the GSM x axis. Their noses are at local noon, and their open ends are at midnight. The magnetopause boundary is therefore a constant λ surface. The constant μ surfaces are paraboloids about the same axis, but with their noses at midnight and their open ends at noon. The third coordinate ϕ is the angle of rotation about the axis of symmetry of the paraboloids, the GSM x axis.

The boundary is defined by its λ coordinate, λ_0, and the focus location. For typically quiet cases, Stern [1985] selected

$$\lambda_0^2 = 11.25 \ R_E$$

$$x_0 = 4.375 \ R_E$$

This surface has its nose at the standoff distance of 10.0 R_E, and its dawn and dusk meridian crossings at 15 R_E from the earth, in agreement with observation [*Fairfield*, 1971].

The finite sum by which the solution is expressed has a finite range of validity A in the μ coordinate. Although the exact solution is an integral over a continuous variable k, the finite sum is obviously more convenient, even though we give up the infinite range of validity. The μ coordinate is zero at the noon crossing of the boundary and increases indefinitely on the night side, where the parabolic shape eventually becomes a poor approximation. Hence there is no point in requiring an infinite range of validity. Typically, $A = 10 \ R_E^{1/2}$ is acceptable. For the choice of $\lambda_0 = 11.25$, this corresponds, from the definition of the parabolic coordinates λ and μ given above, to r = 55.625, x = -45.375.

The boundary condition is that the field lines cannot cross, meaning that the normal component of the total field due to internal and boundary sources must vanish at the boundary:

$$\mathbf{B}_{tot} \bullet \mathbf{n} = (\mathbf{B}_{int} - \nabla V) \bullet \mathbf{n} = 0 \tag{16}$$

where $\mathbf{n}$ is the unit vector normal to the boundary and $\mathbf{B}_{int}$ is the field at the boundary due to the internal sources.

Both the dipole and ring current fields can be decomposed into parts corresponding to orientations of their symmetry axes being parallel and perpendicular to the x_{GSM} axis:

$$\mathbf{B} = \sin \psi \ \mathbf{B}_0 + \cos \psi \ \mathbf{B}_1 \tag{17}$$

10

where ψ is the dipole tilt (For the ring current field this decomposition may not be true in general; it just happens to be true for the Tsyganenko-Usmanov model). The solutions cancelling the normal components of the parallel and perpendicular parts can be obtained separately and then combined to obtain the total solution. The parallel part $\mathbf{B_0}$ is totally symmetric about the GSM x axis; therefore in the corresponding portion of the solution only the m=0 terms are needed. The perpendicular part $\mathbf{B_1}$ separates into the product of $\sin \psi$ and a factor depending only on λ and μ. Therefore for this portion of the solution only the $\sin \psi$ terms are required. The coefficients are obtained numerically by an inversion integral. Typically 10-20 terms are required.

For each new boundary choice the solution must be regenerated. Fortunately there is a scaling law which partially eliminates this requirement. If the boundary is linearly scaled such that a point with Cartesian coordinates (x/k,,y/k,z/k) on the old boundary is transformed to the point (x,y,z) on the new boundary, then the dipole magnetic field at the new boundary is $1/k^3$ times the dipole field at the corresponding point on the old boundary. Therefore the normal component of the dipole field at the new boundary would be canceled by a field equal to $1/k^3$ times the old field at the corresponding point on the old boundary.

We can therefore show that, if V(x,y,z) is the scalar potential for the old boundary field, then

$$V'(x,y,z) = k^{-2}V(x/k,y/k,z/k) \tag{18}$$

is the required scalar potential for the new boundary field. First, the partials of V$'$ may be written, for example,

$$\partial V'/\partial x = k^{-2}(\partial V/\partial x')(\partial x'/\partial x)$$

$$= k^{-3}\,\partial V/\partial x'$$

where x$'$=x/k is the coordinate at the corresponding point. Therefore $\nabla V'$ at the point (x,y,z) is k^{-3} times ∇V at the point (x$'$,y$'$,z$'$), exactly what is needed to satisfy the new boundary condition. Furthermore, since V solves the Laplace equation, it can be readily verified that V$'$ also solves it:

$$\nabla^2 V' = \partial^2 V'/\partial x^2 + \partial^2 V'/\partial y^2 + \partial^2 V'/\partial z^2$$

$$= k^{-4}(\partial V^2/\partial x'^2 + \partial^2 V/\partial y'^2 + \partial^2 V/\partial z'^2)$$

$$= 0$$

Since V$'$ satisfies both the Laplace equation and the new boundary condition, it must be the desired solution.

In terms of the parabolic coordinates the scaling is

$$\lambda_o' = k^{1/2}\lambda_o$$

$$x_0' = kx_0$$

$$V'(\lambda,\mu,\phi) = k^{-2}V(k^{-1/2}\lambda, k^{-1/2}\mu, \phi)$$

11

Viewing V' again as a function of Cartesian coordinates, one finds that

$$\mathbf{B}'(x,y,z) = -\nabla V'(x,y,z)$$

$$= -k^{-3}\nabla V(x',y',z')$$

$$= k^{-3}\mathbf{B}(x',y',z')$$

$$= k^{-3}\mathbf{B}(x/k,y/k,z/k) \qquad (19)$$

This is the same scaling law as that used in the Olson-Pfitzer dynamic model, where, in that model, $k = (R_{st}/10.5)$.

The ring current scaling is similar, except that the ring current parameter ρ_0 must undergo the scaling

$$\rho_0' = k\rho_0$$

at constant $B_0\rho_0^3$, where B_0 is the ring current strength parameter, in order that its magnetic field at the new boundary be equal to k^{-3} times its field at the old boundary, in the same way as for the dipole field. Then we would obtain the analogous relation

$$V'(x,y,z; B_0 k^{-3}, k\rho_0) = k^{-2}V(x/k,y/k,z/k; B_0, \rho_0)$$

where V' is the scalar potential for the new boundary in the presence of a ring current parameterized by $k\rho_0$, while V is the potential for the old boundary in the presence of the original ring current with parameter ρ_0. The new boundary solution, in the presence of the original ring current is therefore:

$$V'(x,y,z; B_0,\rho_0) = k^{-2}V(x/k,y/k,z/k; k^3 B_0, \rho_0/k) \qquad (20)$$

The scaling law therefore doesn't seem to help us here, since a boundary change of scale would still require a new calculation of the coefficients associated with the new value of ρ_0. However, as a tabulation of these coefficients as functions of ρ_0 is generally available anyway, for studies related to the variations of the ring current, little new computation effort would likely be required.

If the finiteness of ρ_0 can be neglected, that is, the dependence of the magnetopause field on ρ_0, for fixed $B_0\rho_0^3$, can be neglected (either small B_0 or small variation of k from unity), we may recover the simple scaling law, Eq. (19), as an approximation to Eq. (20).

2.5.2 Stretched Magnetosphere Model

The magnetotail currents generally cause the nightside field lines to stretch in the tailward direction. This motivated Stern [1987] to develop an explicit model of this stretching, rather than to build a model from assumed currents. In the stretched magnetosphere model, the dipole + ring + tail field is represented by:

$$B_x{}'(x,y,z) = B_x(f(x),y,z) \tag{21a}$$

$$B_y{}'(x,y,z) = f'(x)\, B_x(f(x),y,z) \tag{21b}$$

$$B_z{}'(x,y,z) = f'(x)\, B_z(f(x),y,z) \tag{21c}$$

where $f(x)$ is a stretch function, $f' = df/dx$, B_x, B_y, and B_z, are the GSM components of the dipole + ring field, and x, y, and z are the GSM coordinates. Since the stretched field was derived as the curl of another vector, it is therefore divergence-free. The published stretch function is a tabulation out to 25 R_E, chosen so that the night side equatorial field intensity fits the observations of Fairfield [1968]. The inner boundary of the stretching is 5 R_E down the tail. Sunward of this the field is not stretched.

The author has supplied us with a revised stretch function (Table 2), which we have used in this report. In this model the inner boundary is 1.5 R_E down the tail.

Table 2. Revised Stretch Function

$x_{GSM}(R_E)$	$f(x)$	$f'(x)$
-1.5	-1.5	1.000
-2.0	-1.999	0.991
-3.0	-2.964	0.930
-3.5	-3.416	0.873
-4.5	-4.212	0.711
-5.5	-4.831	0.525
-6.5	-5.266	0.349
-7.5	-5.539	0.205
-8.5	-5.697	0.120
-9.5	-5.785	0.059
-11.0	-5.841	0.024
-13.0	-5.864	0.001
-15.0	-5.857	-0.005
-25.0	-5.823	-0.000

Although the magnetopause field scaling laws mentioned earlier do not hold precisely for the stretched magnetosphere, tests have indicated errors less than 1 nT arise if the standoff distance varies less than 20 percent from the standard quiet model value, 10 R_E.

13

3. SOFTWARE

The software package OPTRACE [*Radex, Inc.,* 1987; *Jordan and Bass,* 1989] was adapted for the work reported here. The new version, called BFLDSM, computes the model magnetic field vector and McIlwain L parameter [*McIlwain,* 1961] in the same way as OPTRACE. The external field model is computed by a subroutine BXYZMU, a version of which exists for each of the models. Thus, to use a particular model, the version of BXYZMU which calculates that model must be loaded with the rest of the code. The Tsyganenko, Tsyganenko-Usmanov, and Stern model codes were provided by D. P. Stern. The Olson-Pfitzer codes were supplied by Olson and Pfitzer. The Mead-Fairfield code was written by Radex.

The internal field predominantly used was the IGRF85 model, with maximum degree of 10. However, on occasion we have used others, loading the appropriate routine as for the external model.

Table 3 lists the VAX 8650 computation time per 10000 subroutine calls for the various external models and the IGRF85 internal model. The table shows that the time for a total internal + external model calculation is not terribly sensitive to the choice of external model, unless the external model is Sterns's. Most of the Stern model computation time is in the magnetopause part, which requires generation of Bessel functions for the parabolic harmonic expansions, which were truncated at n=5. The Bessel functions were computed with routines from Press, et al. [1986].

Table 3. Vax 8650 Computation Times (sec/10000 calls)

Olson-Pfitzer Tilt Dependent	2.0
Olson-Pfitzer Dynamic	5.2
Mead-Fairfield	0.3
Tsyganenko-Usmanov	1.8
Tsyganenko Short Version	3.0
Tsyganenko Long Version	3.6
Stern Parabolic Magnetopause/ Stretched Magnetosphere	12.0
IGRF85	9.2

Several options have been added to BFLDSM. These include the option to input the point at which the field and L are to be computed in solar magnetic or geocentric solar magnetospheric coordinates, rather than geographic; the option to truncate the internal model; and the option to fix the dipole tilt and the solar magnetic longitude.

4. L PARAMETER COMPARISONS

As explained by Jordan and Bass [1989], the McIlwain L parameter [*McIlwain*, 1961] at a point is a function of the first two adiabatic invariants of particles mirroring at that point, provided the magnetic field is static. For internal fields we may consider this to be true if we neglect the slow secular change known to be taking place. Also for internal fields the L parameter is approximately equal to the radial distance, in R_E, of the equatorial crossing of the field line through the point in question. In Figures 1-4 we show $\Delta L = L - L_d$, where L_d is the dipole parameter, $r/\sin^2\theta$, with θ the magnetic colatitude, and r the radial distance of the point in R_E. The characterization of L_d as the "dipole" L parameter follows from the equation for the dipole field line

$$r = L_d \sin^2\theta \qquad (22)$$

with L_d the radial distance to the equatorial crossing of the field line. Thus L_d is the L parameter of the point in a dipole field of magnetic moment M equal to that used in the definition of L (see Jordan and Bass [1989]). In the figures we show contours of constantΔL for the IGRF85 model, updated to 1 Jan. 1990. The individual contour plots are at designated values of L_d, and are on magnetic latitude-local time grids. The dipole tilt is zero, meaning that the dipole vector is normal to the earth-sun line, and the solar magnetic longitude (SLON) is zero. The contours cover only locations above the surface of the earth. Thus, as L_d increases, the amount of latitude space covered increases.

Near the equator ΔL is less than 0.1, but it exceeds this value in the South Atlantic Anomaly and at high latitudes. As L_d increases, $\Delta L = 1$ contours appear at the high latitudes, which were below the surface at lower L_d. One remarkable feature that appears is that a contour is nearly stationary beyond the L_d threshold for its appearance; thus ΔL is approximately independent of L_d.

Figures 5-8 similarly display ΔL for a field composed of the IGRF85 internal model and the Olson-Pfitzer tilt dependent external model. In Figs. 6-8 we have marked the local minima and maxima with "L" and "H", repectively, indicating their values. Now, as L_d increases, the contour pattern begins to deviate substantially from the IGRF85 baseline. At high L_d there is a large area around the sub-solar point with $\Delta L < -1$, and a corresponding area around the anti-solar point with $\Delta L > 1$.

To examine this effect further, and in particular to more easily compare the models, we have plotted in Figures 9 and 10 ΔL vs L_d at 0° and 20° dipole latitude, respectively, for both noon and midnight, and for 0° and 18° dipole tilt. The latitudes and radial range were chosen to reflect the planned CRRES orbital parameter ranges. We compare in these figures the IGRF85 model alone ("NO Ext", solid line) with results obtained for IGRF85 + Tsyganenko-Usmanov, Tsyganenko short version ("Tsyg" 1987), Mead-Fairfield, and Olson-Pfitzer tilt-dependent models. The constant and very low ΔL for the internal model alone is in agreement with what was observed in the contours plots. One readily sees the growing effect of the external models as L_d increases. A radiation belt particle which mirrors at the equator (equatorial pitch angle = 90°) must follow a path of constant L. At noon the $L = L_d$ path is outside the $L_d = $ constant circle by approximatly the amount shown in the noon plot. Thus at noon the L=7 path is approximately 0.5 R_E outside the $L_d = 7$ circle. At midnight nearly the opposite is true: The L=7 path is inside the $L_d = 7$ circle. Thus a trapped particle conserving its adiabatic invariants and mirroring at the equator travels a path significantly distorted from a circular path.
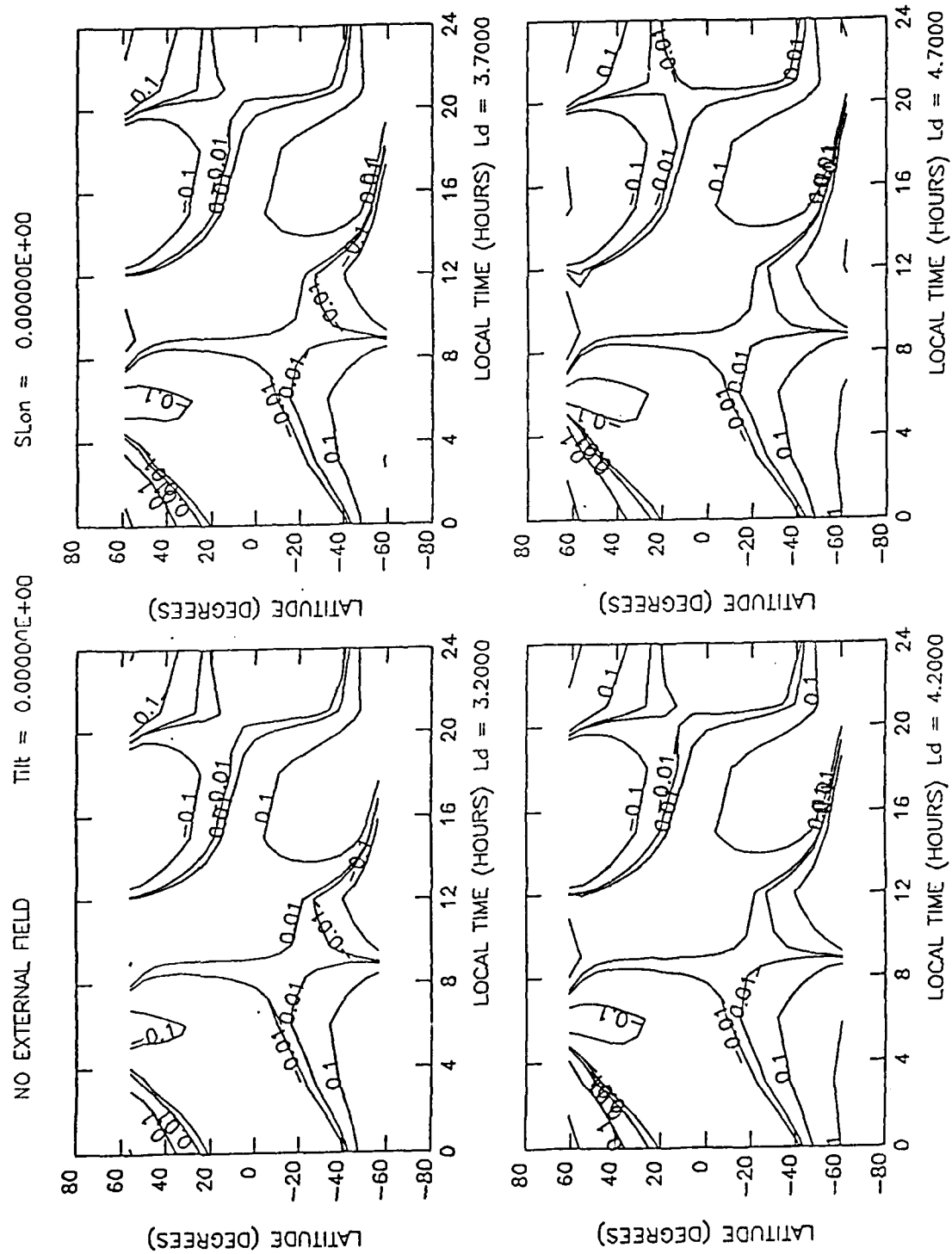
15

NO EXTERNAL FIELD   Tilt = 0.00000E+00   SLon = 0.00000E+00

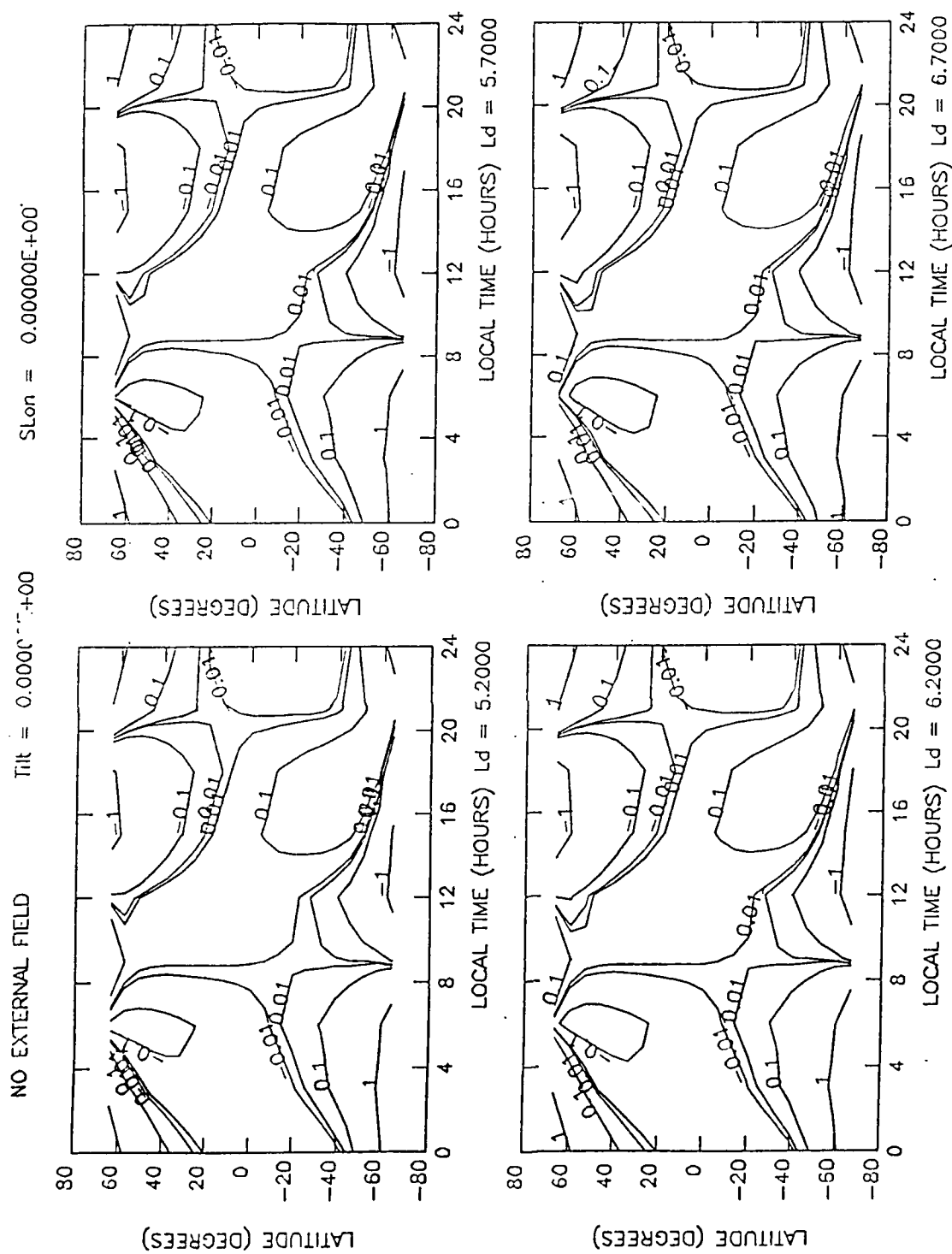Figure 1. Contours of constant $\Delta L = L - L_d$: internal magnetic field; L_d = 3.2, 3.7, 4.2, and 4.7.

16

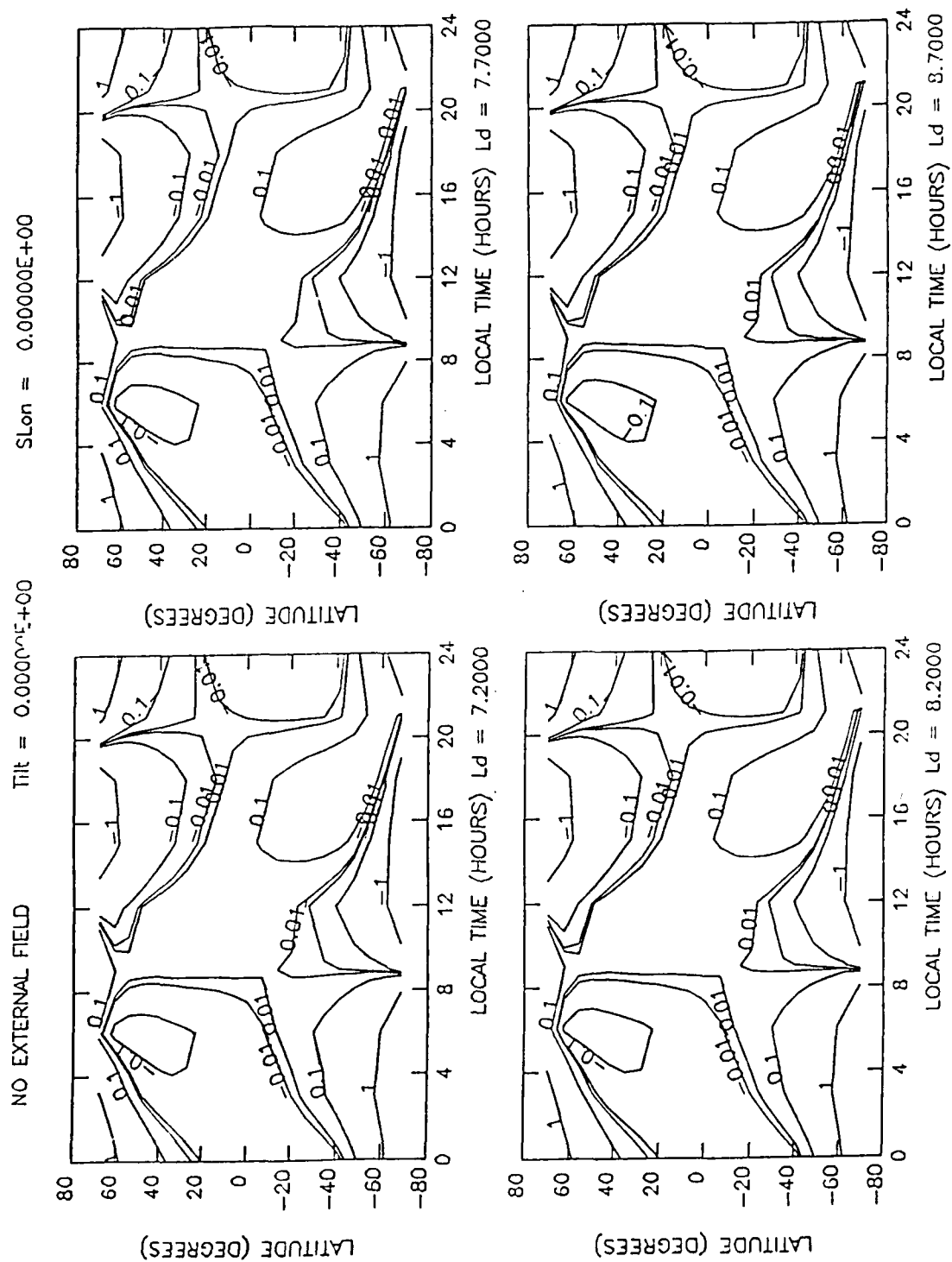Figure 2. Same as Figure 1, but for L_d = 5.2, 5.7, 6.2, and 6.7.

17

Figure 3. Same as Figure 1, but for L_d = 7.2, 7.7, 8.2, and 8.7.

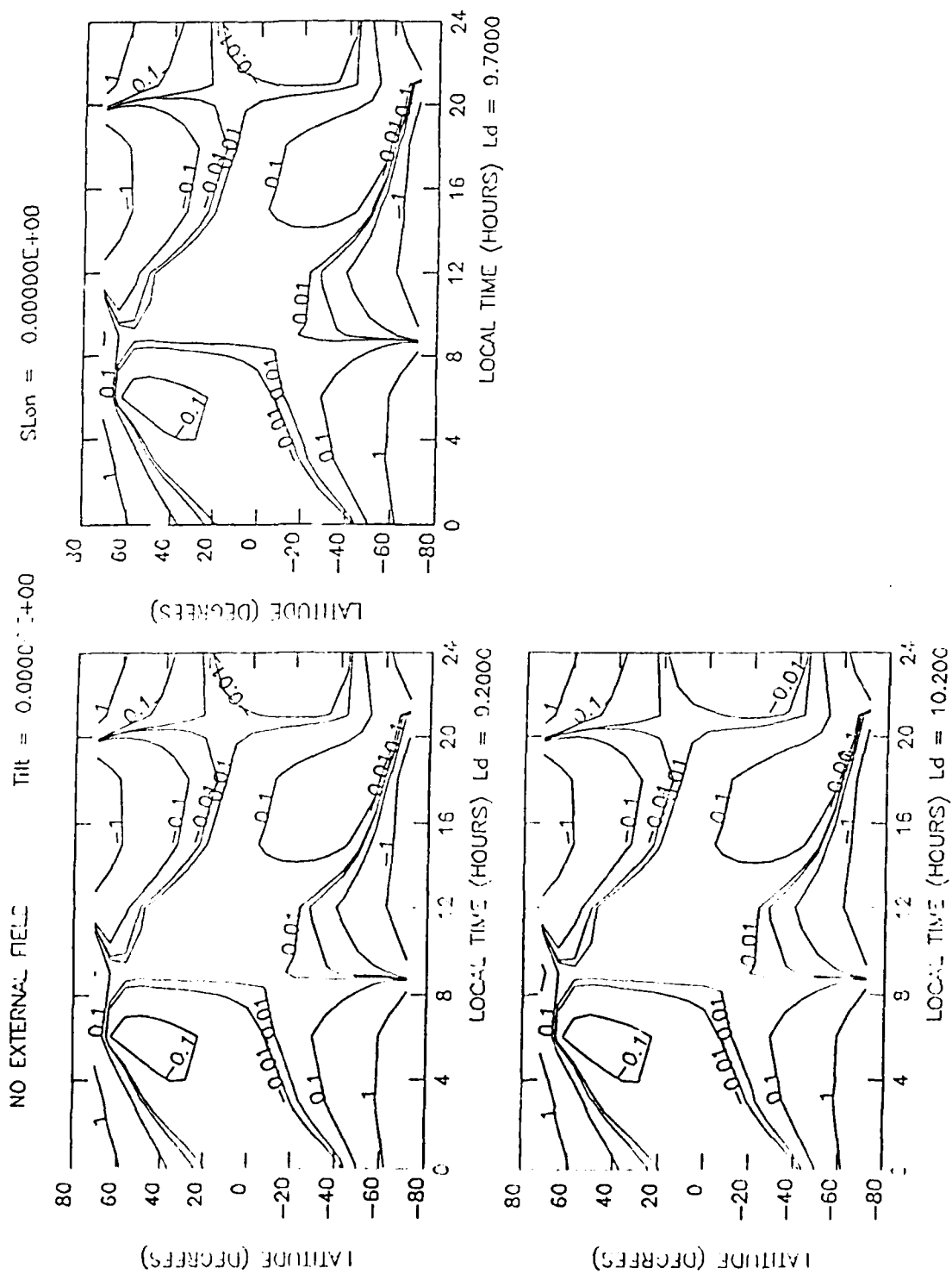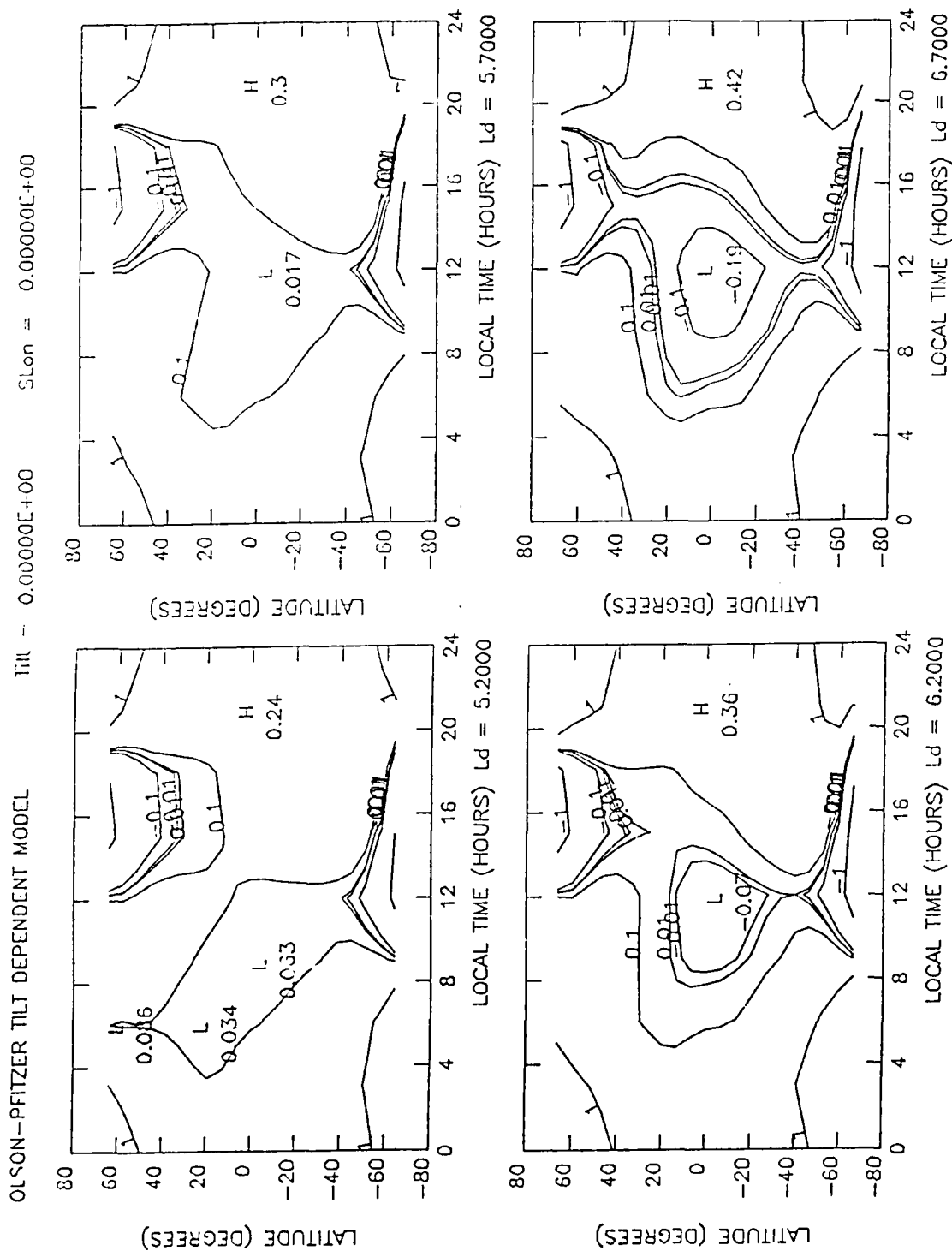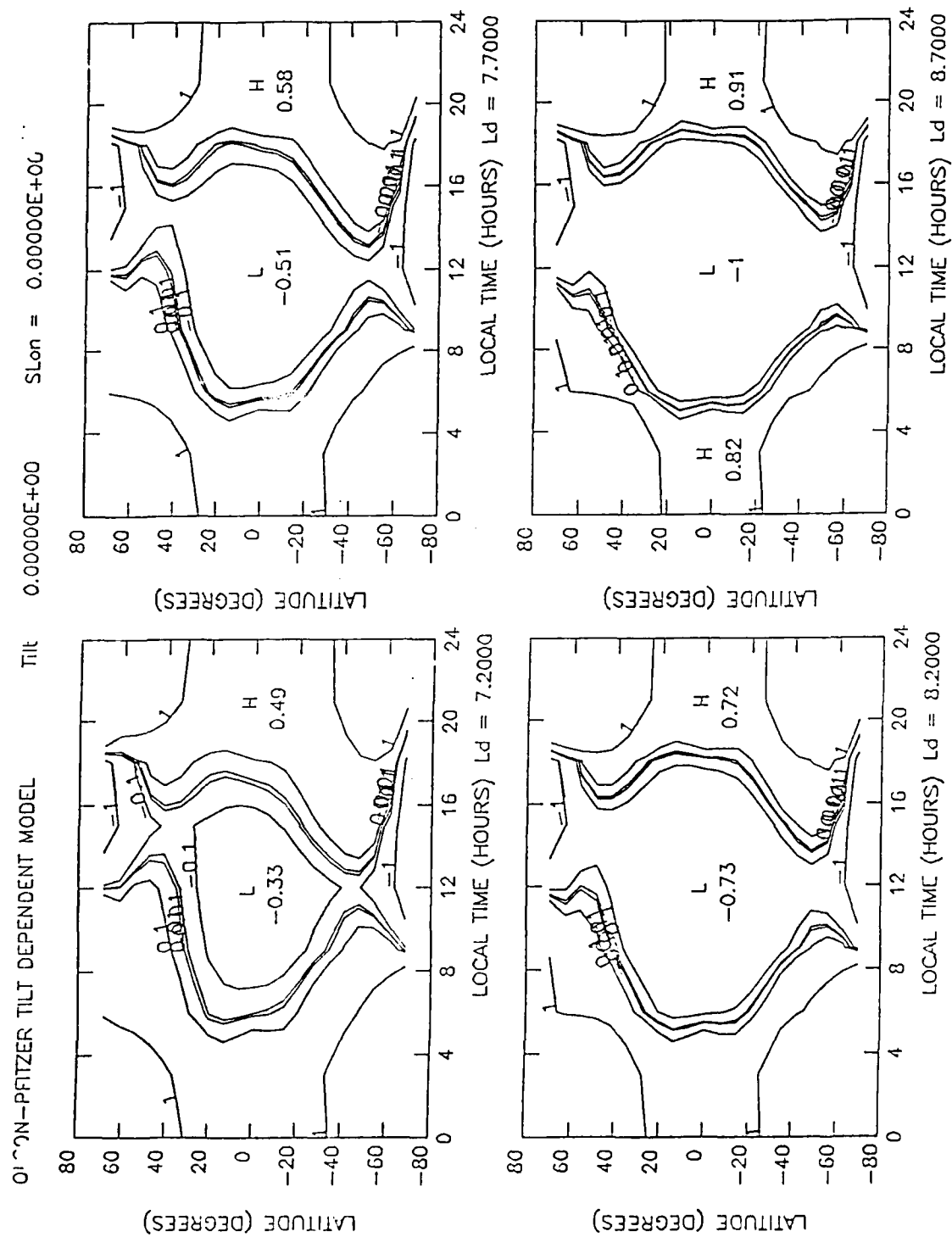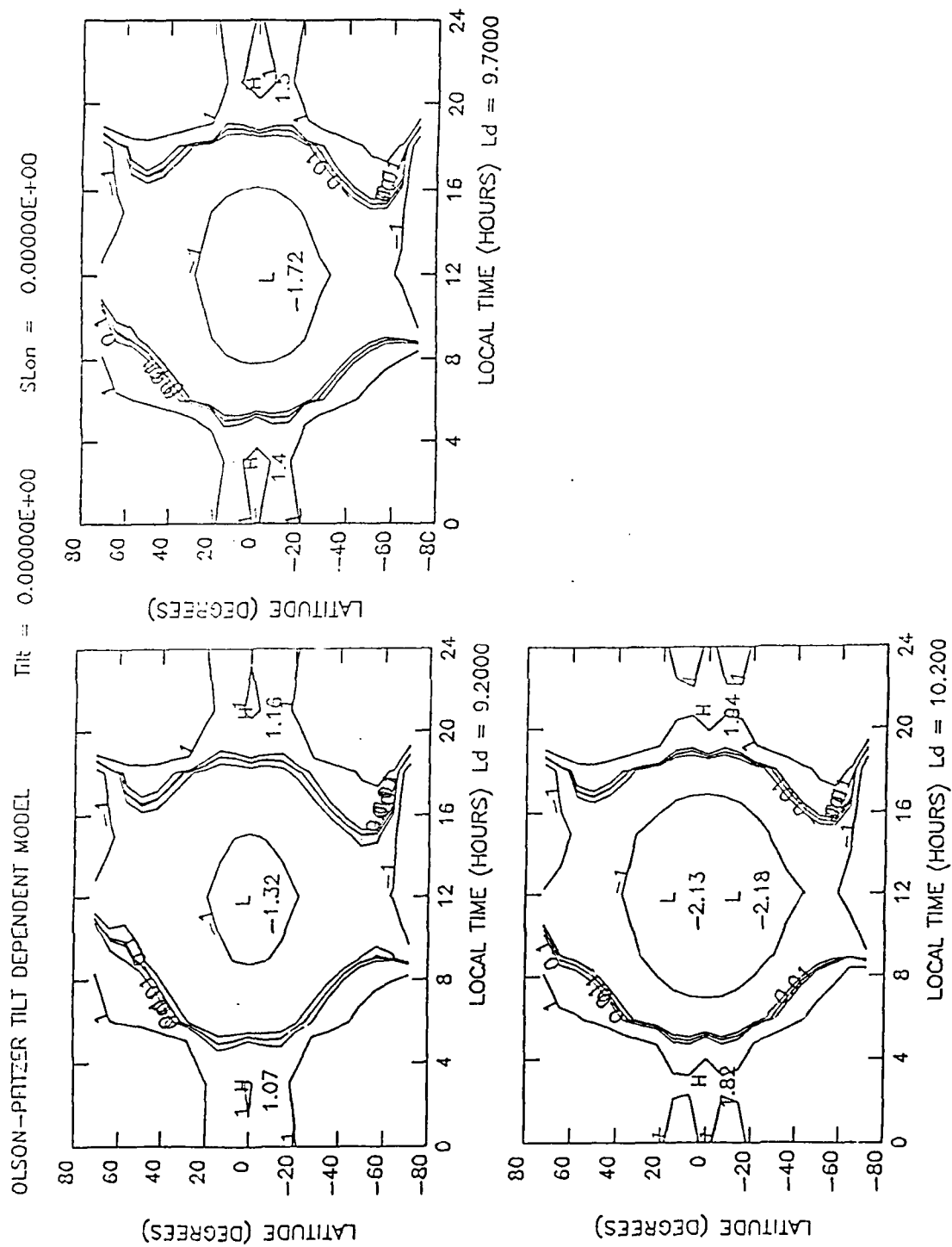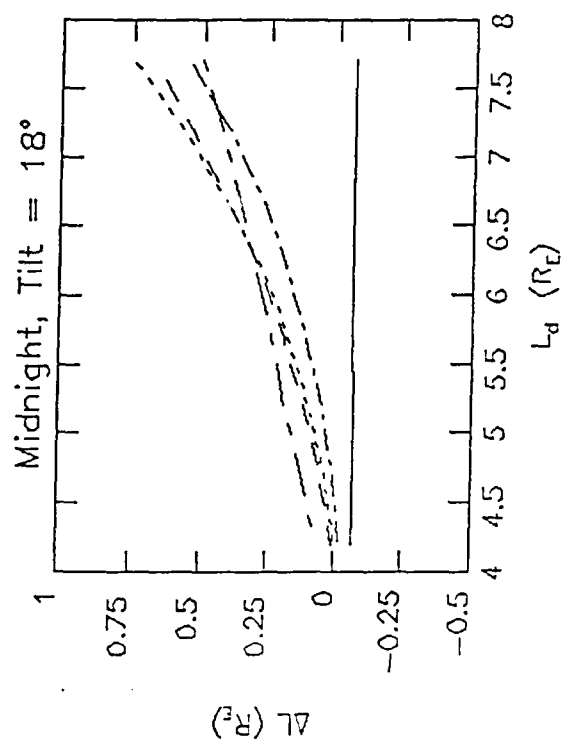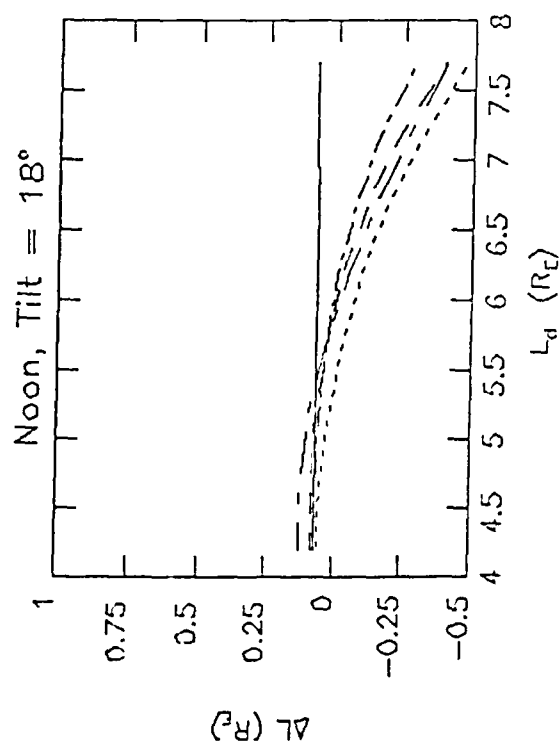Figure 4. Same as Figure 1, but for $L_d = 9.2$, 9.7, and 10.2.

19

Figure 5. Same as Figure 1, but for internal model + Olson-Pfitzer tilt dependent external model.

Figure 6. Same as Figure 5, but for L_d = 5.2, 5.7, 6.2, and 6.7.

21

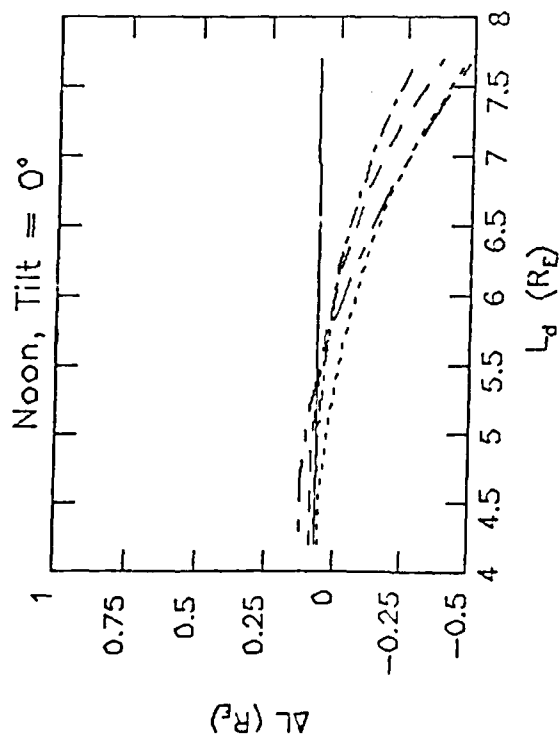Figure 7. Same as Figure 5, but for L_d = 7.2, 7.7, 8.2, and 8.7.

22

Figure 8. Same as Figure 5, but for L_d = 9.2, 9.7, and 10.2.
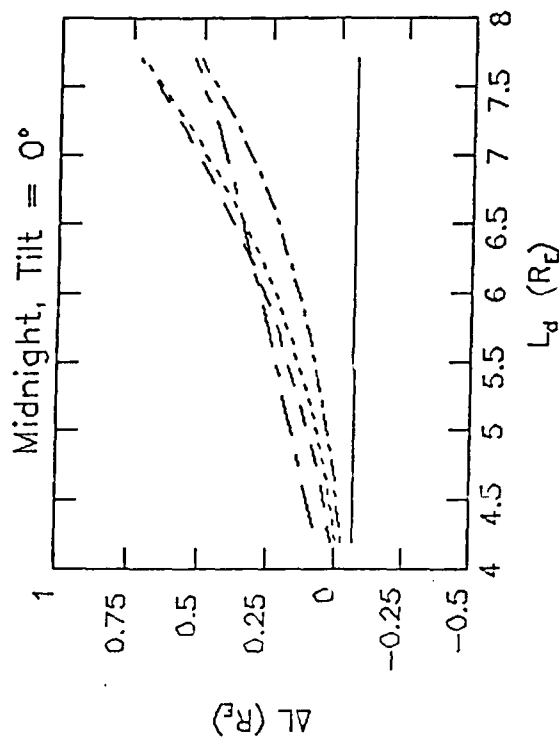
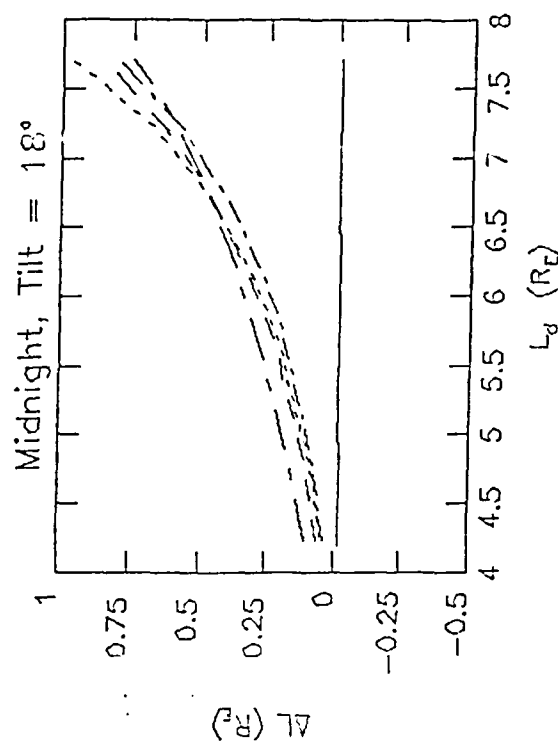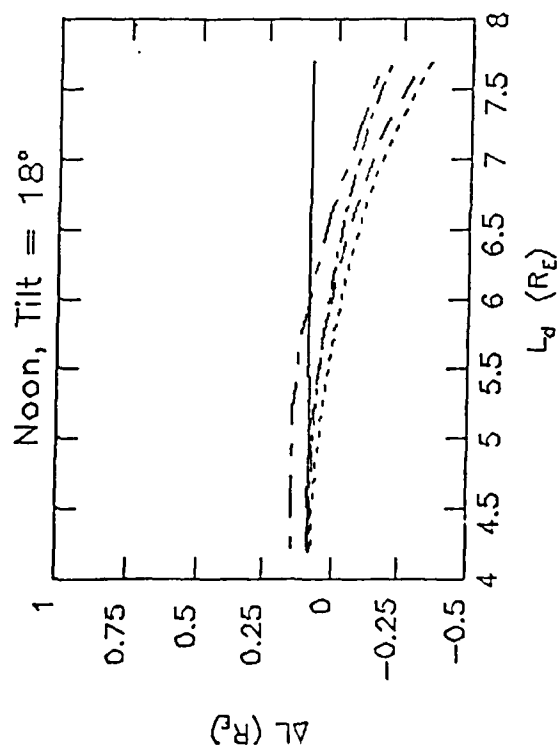Figure 9. Noon and midnight equatorial ΔL profiles for $K_p = 0$
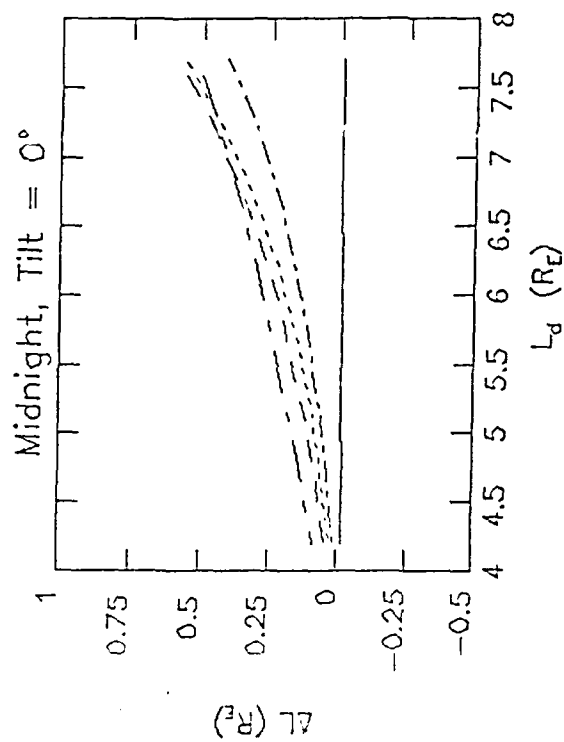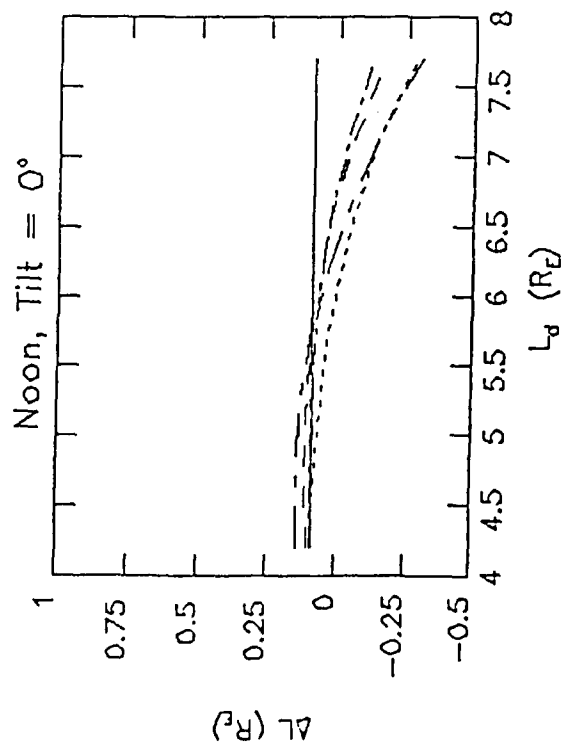
Figure 10. Same as Figure 9, but for 20°N magnetic latitude.

The differences between the models is up to 0.25 R_E in the high L_d region of the plots. The Olson-Pfitzer tilt-dependent model yields the largest L values in the inner region, while the Mead-Fairfield model gives the largest values in the outer region at noon, and the Tsyganenko and Tsyganenko-Usmanov models yield the largest values at midnight. The Olson-Pfitzer midnight L increases nearly linearly with distance, while the L values for the other models increase more rapidly in the outer region than in the inner region.

The dependence of the L value on dipole tilt is negligible at the equator, but significant at 20° latitude. Figure 11 highlights the tilt dependence of the midnight L values at 20° latitude.

We thus see that there are substantial modifications in the trapped particle orbits when the external field is introduced, and noticeable differences between various models of the external field. Thus it is worthwhile to compare the models with observations.
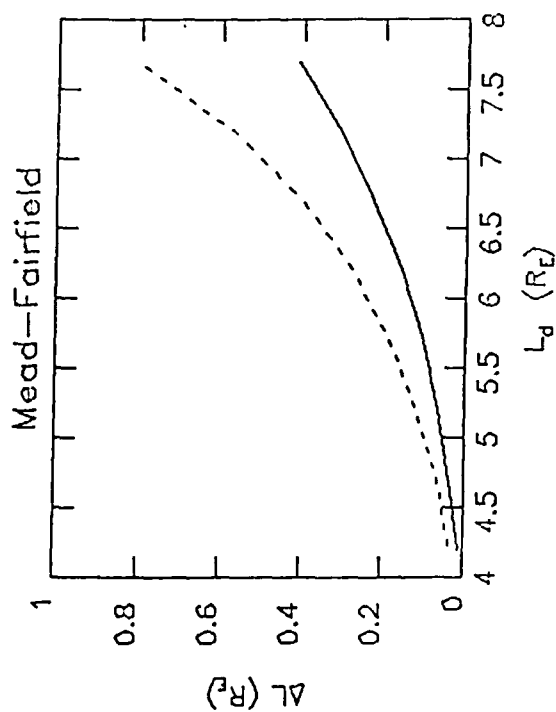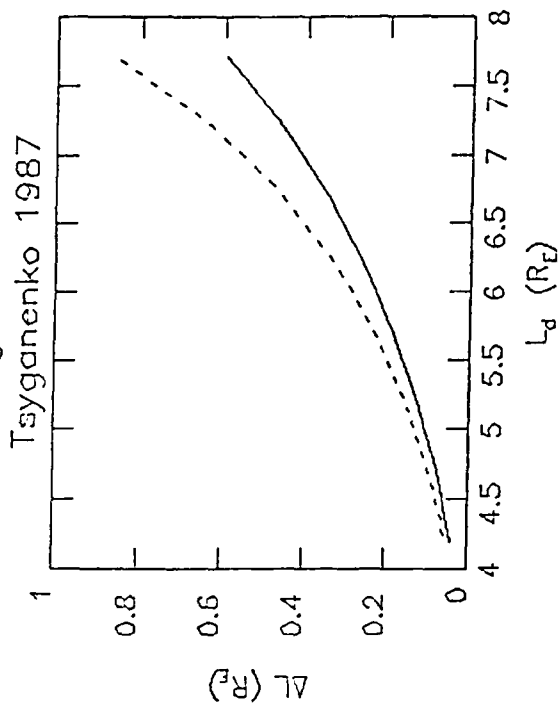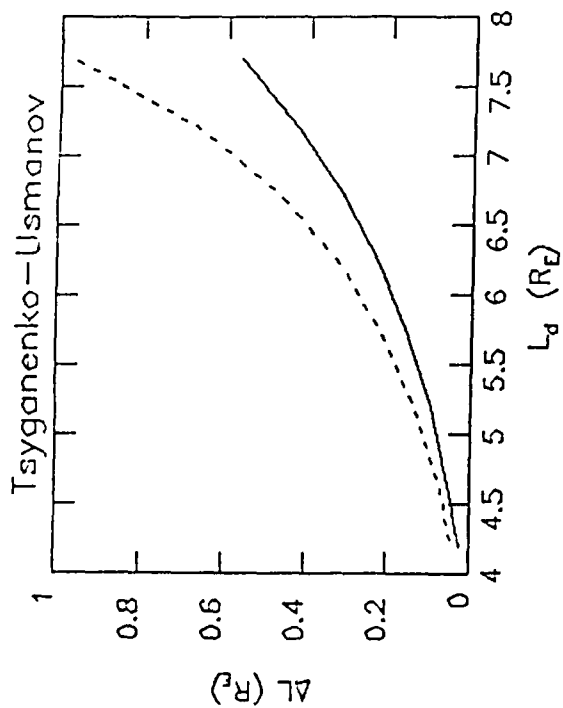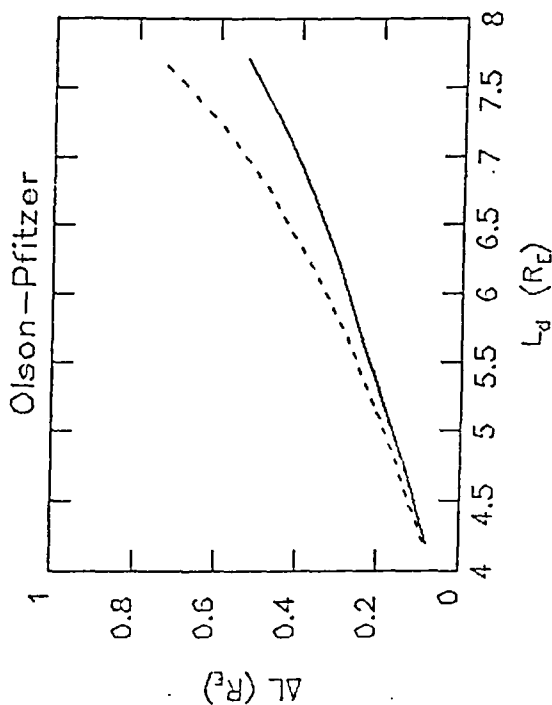
Figure 11. Tilt dependence of L at midnight, 20° latitude

5. MODELS VS. DATA

A static radiation belt model will require a good static magnetic field model. Therefore we have chosen SCATHA magnetometer data from the magnetically quiet 20 April, 1979, for comparison with the models. Despite the quiet condition, the solar wind pressure increased steadily during the period, allowing us to test the magnetopause modeling capabilities of the various models. The following day there was a small substorm, during which the measured magnetic field magnitude decreased considerably from the prediction of the static Olson-Pfitzer tilt dependent model. If we wish to model adiabatic variations of the radiation belt particles during such substorms, we need to have an accurate model of the magnetic field variations.

Since the SCATHA orbit is limited to the outer belt, we also examined some published AMPTE/CCE results [*Fairfield, et. al.,* 1987]. As argued by these authors, the inner magnetic flux has a bearing on the equatorial crossings of magnetic field lines intersecting the Earth's surface at given latitudes: the flux intersecting the surface equatorward of a field line in a specified longitudinal sector is approximately equal to the flux intersecting the equator in the same sector earthward of the equatorial intersection of the field line.

5.1 COMPARISONS OF MODELS WITH SCATHA DATA

The SCATHA satellite orbit is a 5.3 R_E x 7.8 R_E low inclination (7.9°) near-geosynchronous orbit with an easterly drift rate of about 5° per day. On 20 April, 1979, the perigee of the SCATHA orbit was at 1600 hours MLT, the apogee was at 0300 hours MLT, and the magnetic latitude was within ±4.5°. The magnetometer data used in the following were averaged over 1/20 R_E bins (~ 15 min.).

Figure 12 shows a comparison of measured magnetic field magnitudes for this day with the predictions of various models. The Olson-Pfitzer dynamic model was computed using the hourly DST, solar wind speed, and solar wind ion number densities available on the NASA NSSDC online data OMNI data base. The magnetopause and tail strengths and dimensions were scaled in accordance with the discussion in section 2. The Tsyganenko 87 (short version), Tsyganenko-Usmanov, and Mead-Fairfield models were computed with the three-hourly K_p values. The internal model was the Barraclough 1975, updated to the date in question. Perigee occurs at maximum field strength, ~ 3 hours UT, while apogee occurs at minimum field strength, ~ 13 hours UT. The models follow the data quite well; the principle area of disagreement is at perigee, where the models all predict higher values than measured.

Figure 13 shows the difference between the measured and modeled field on an expanded scale for this day. We have also added Stern's model, assuming, for the ring current field, $\rho_0 = 4 R_E$, and $B_0 = -20$ nT. The magnetopause field was computed from a baseline field for 10 R_E standoff distance, using the simple scaling law Eq. (19), with k = $R_{st}/10.0$, where R_{st} is computed from Eq. (6). For the given ring current parameters, and the standoff distance for this period (Fig. 14), the error in using the simple scaling law, which neglects the finiteness of ρ_0, is less than 0.3 nT.

Of all the models, the Stern model disagrees the most with the data, while the Olson-Pfitzer dynamic model agreement is generally the best, particularly at perigee, where the differences are greatest. With the exception of the Stern and Olson-Pfitzer dynamic models, the differences at the end of the day, as the next perigee is approached, are positive, opposite in sign from the differences at the beginning of the day, at the same location in the orbit. Thus the field seems to
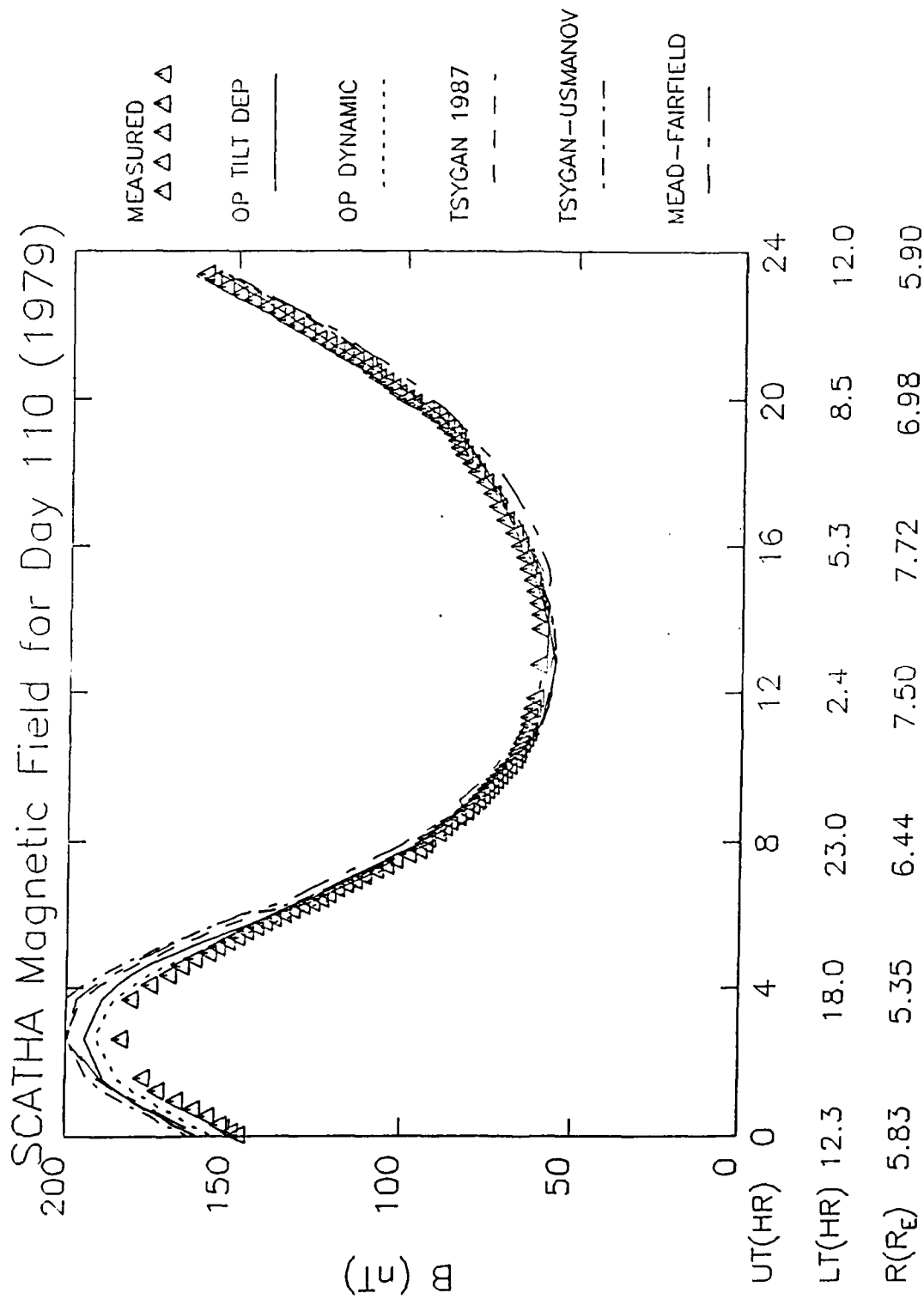
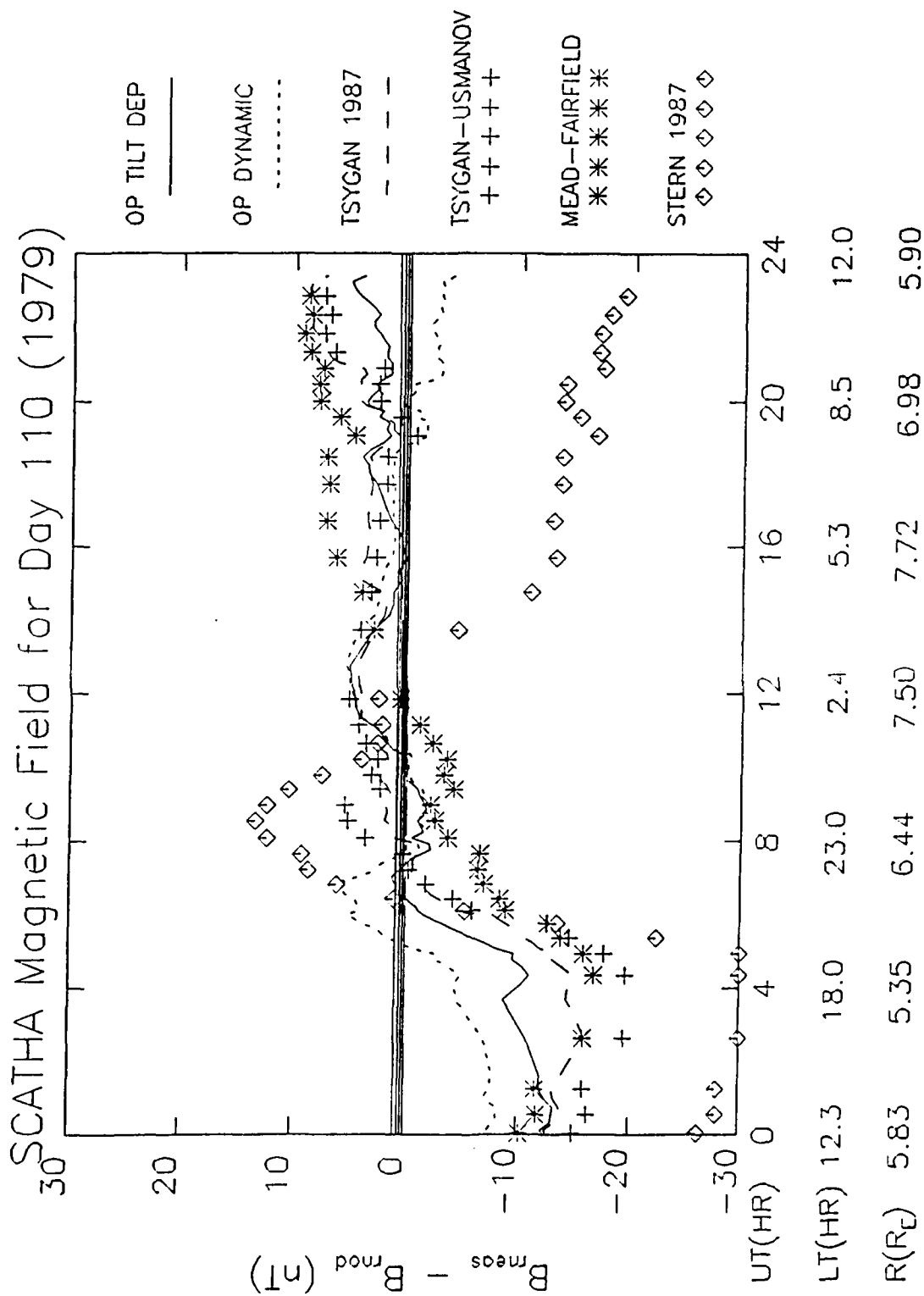Figure 12. Measured (SCATHA) and model field intensity: 20 April, 1979.

Figure 13. Measured - model differences: 20 April, 1979

30

have increased over the 24 hour period relative to the models. In fact, the standoff distance implied by the the solar wind data decreased steadily during the day (Fig. 14). Thus, it appears that the Olson-dynamic and the Stern models, with their explicit dependence on the standoff distance, depict this variation better than do the other models.

The comparatively large deviations of the Stern model are not surprising, since that model has not been extensively fit to data. The large negative deviations for the day local times (meaning the model field intensity exceeds the measured) could possibly be improved by increasing the ring current, but this would worsen the disagreement of opposite sign at night local times. The stretch function evidently overestimates field line stretching for this case of extremely low activity.

Figure 15 shows the measured and model magnetic field magnitudes for the next day, 21 April, 1979. On that day a substorm occurred with growth phase commencing at ~ 5 hours UT. The measured magnetic field is seen to decrease significantly with respect to all the models. Initially the Olson-Pfitzer dynamic model seems to follow the data marginally better than the other models, but that may only be because it uses hourly indices, while the other dynamic models use the 3-hourly K_p. Thus, later on the others are doing just as well. On the expanded scale difference plot (Fig. 16), the start of the substorm is indicated by the sharp drop in the measured minus Olson-Pfitzer static model difference (solid line) at ~ 4-5 hours UT. During this period, the measured Olson-Pfitzer dynamic model difference (dotted line) actually increases, meaning that the dynamic model depicted a faster decrease than was observed. Later, however, the Olson-Pfitzer dynamic model is almost as far off the data as the others. During subsequent disturbances on that day, no model does outstandingly well.

While one would not expect the models to match such nearly instantaneous variations in the actual field, one would hope that ultimately, they would "catch up", i. e. the delay in the model response time could simply be due to the time resolution of the index used, particularly the case for K_p. The fact that the models continue to vary smoothly, well beyond the abrupt change shown in the data, indicates that this is not the case. It is possible that the K_p dependent models suffer simply because K_p is not adequately sensitive to the variations of the field. The Olson-Pfitzer dynamic model is driven by parameters more directly tied to the physical processes which determine the magnetic field's configuration. These parameters, which are available in one hour resolution as opposed to K_p's three hour resolution, include DST (a measure of the ring current) and the solar wind pressure and speed (which determine the noon magnetopause standoff distance input directly to the model). However, a probable oversimplification in the model is that the tail current variation is determined purely by the magnetopause scaling.

5.2 MIDNIGHT EQUATORIAL FIELD STRENGTH DEPRESSION

One important feature of the magnetic field is the variation of the field magnitude along the equator in the noon-midnight plane. On the midnight side the external sources generally cause a depression in the total field strength, stretching tailward the field lines connected to given locations on the Earth's surface. Therefore, as pointed out by Fairfield, et. al. [1987], the magnetic mapping of given points on the Earth's surface to the equator is determined by the amount of this depression. Thus, an accurate model of the midnight equatorial depression is needed to relate auroral observations, such as precipitation boundaries and field aligned currents, to high latitude equatorial factors such as convection, injections, and plasma pressure gradients.

Figure 17 compares averaged observed equatorial midnight field depressions, adopted from Fairfield, et. al. [1987], for various K_p bins with those predicted by the models. The 0-1 bin and the 2-3 bin are from Sugiura and Poros [1973], based on OGO measurements, while the results

31
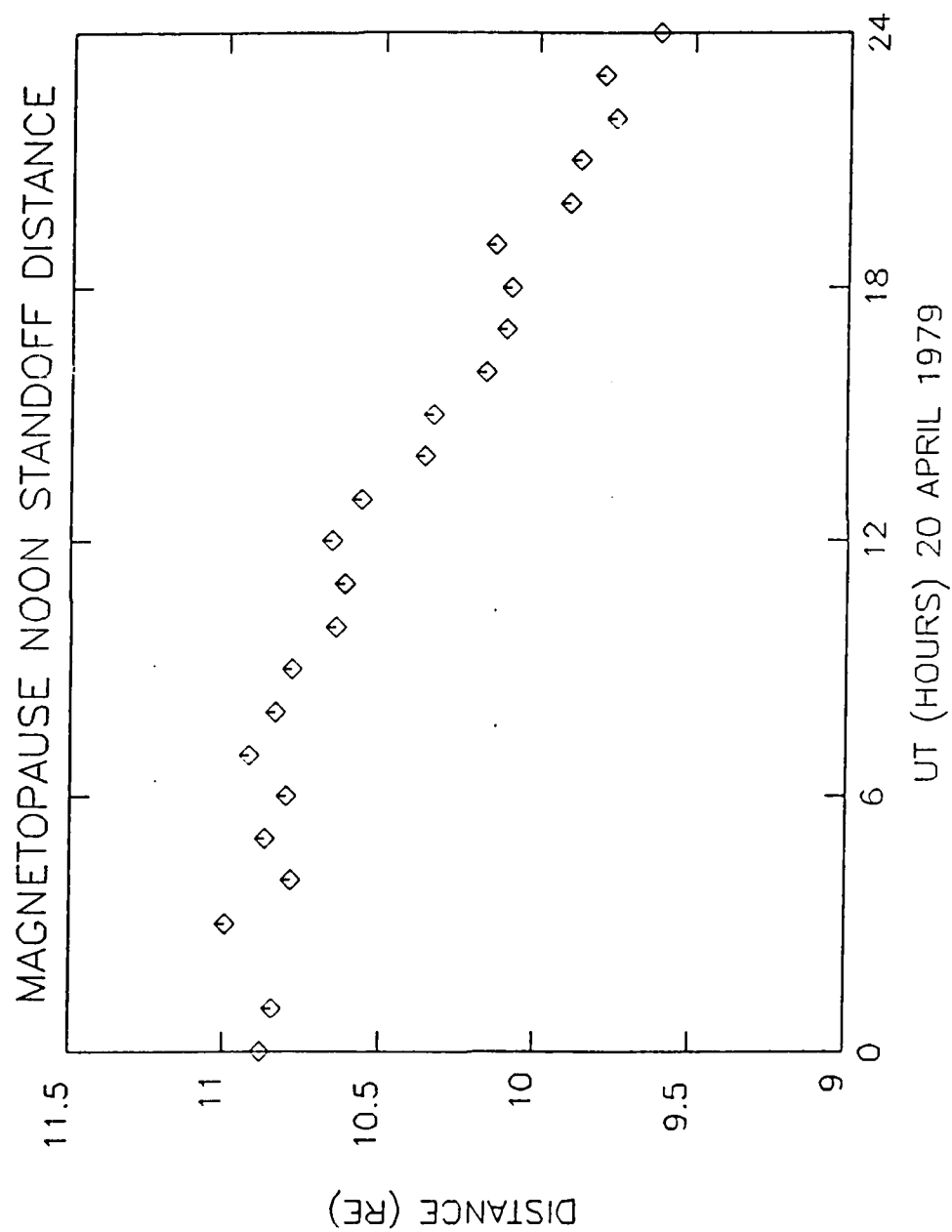
Figure 14. Noon magnetopause standoff distance: 20 April, 1979.
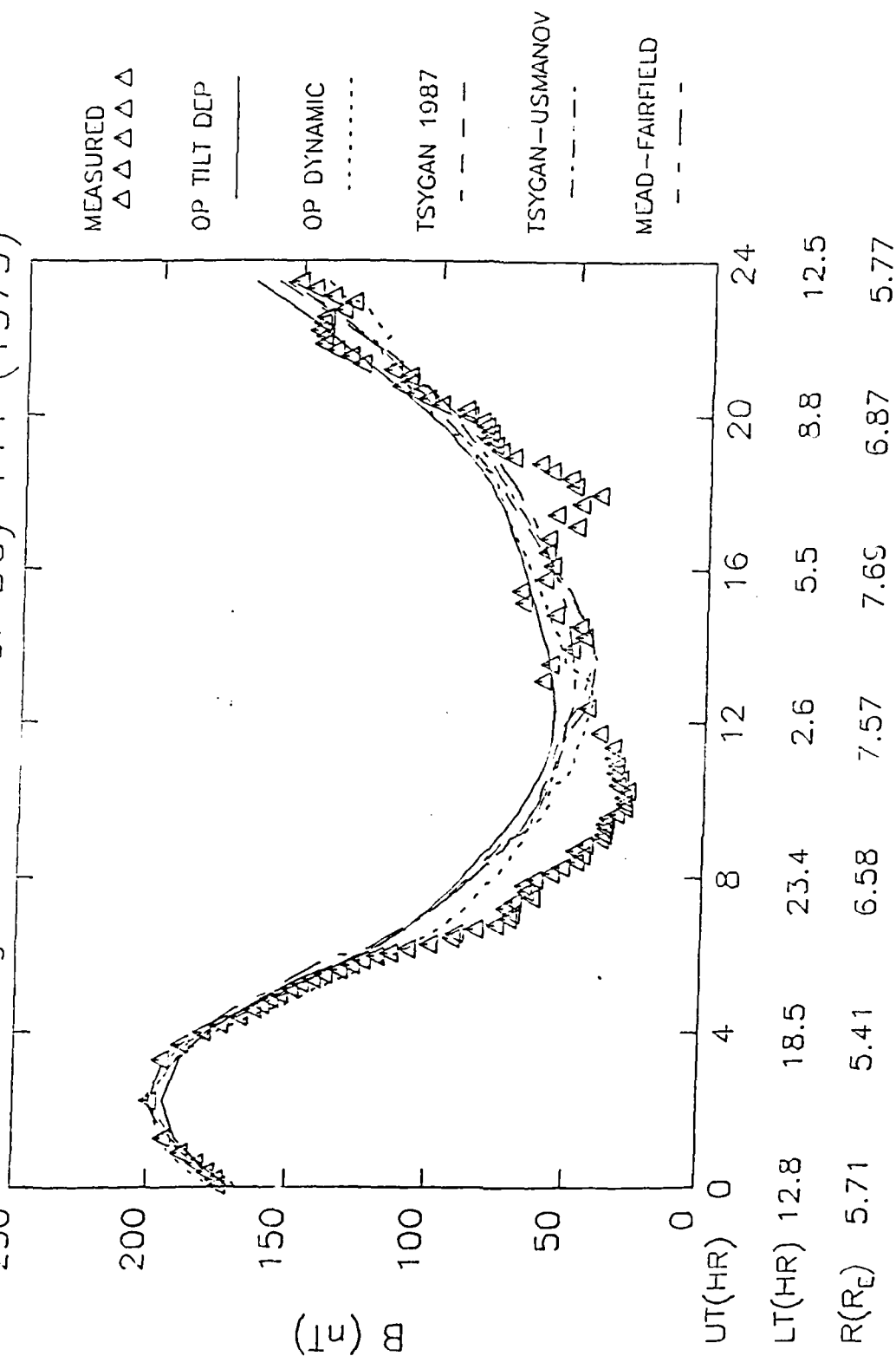
Figure 15. Same as Figure 12, but for 21 April, 1979.

33
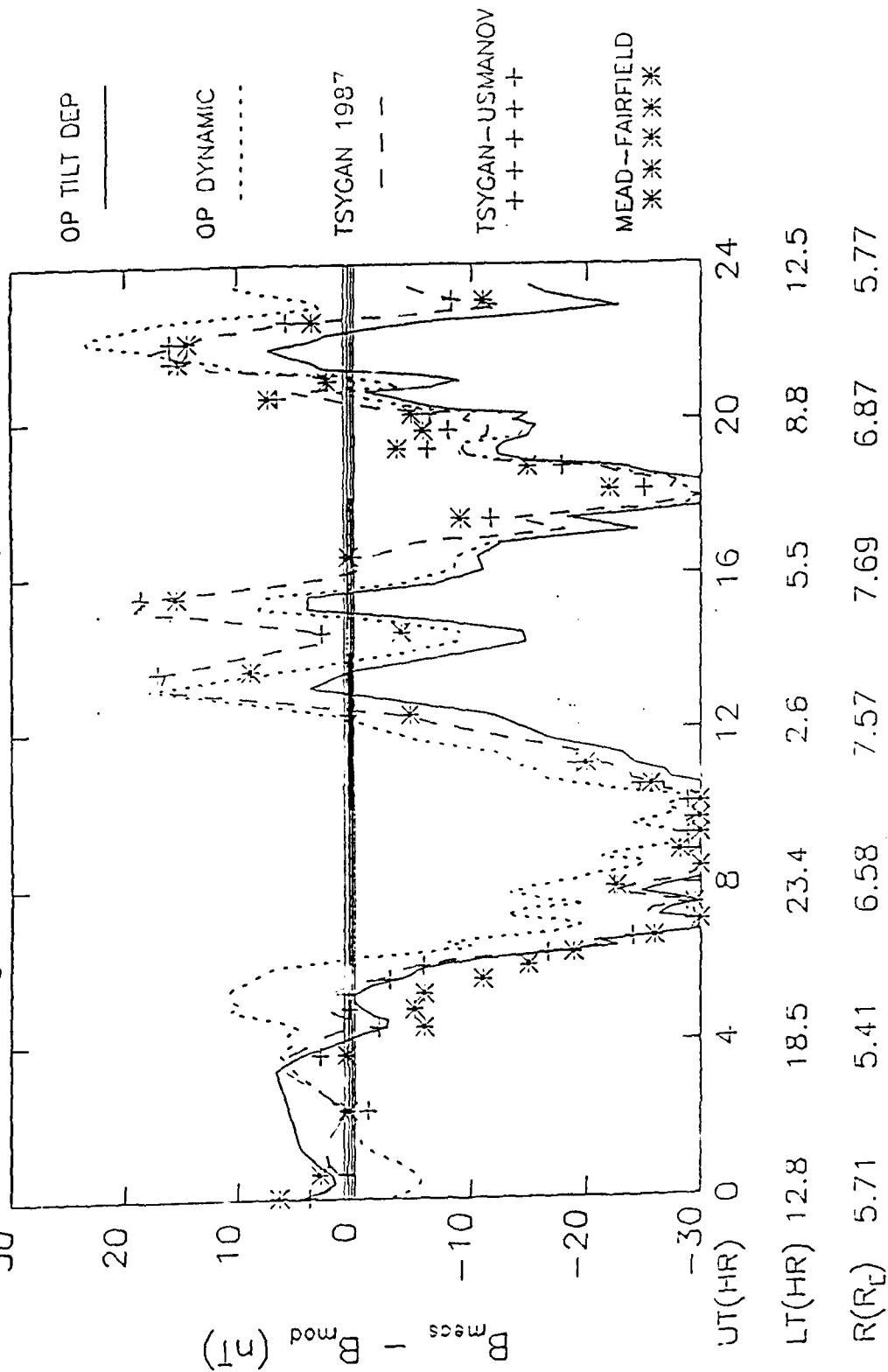
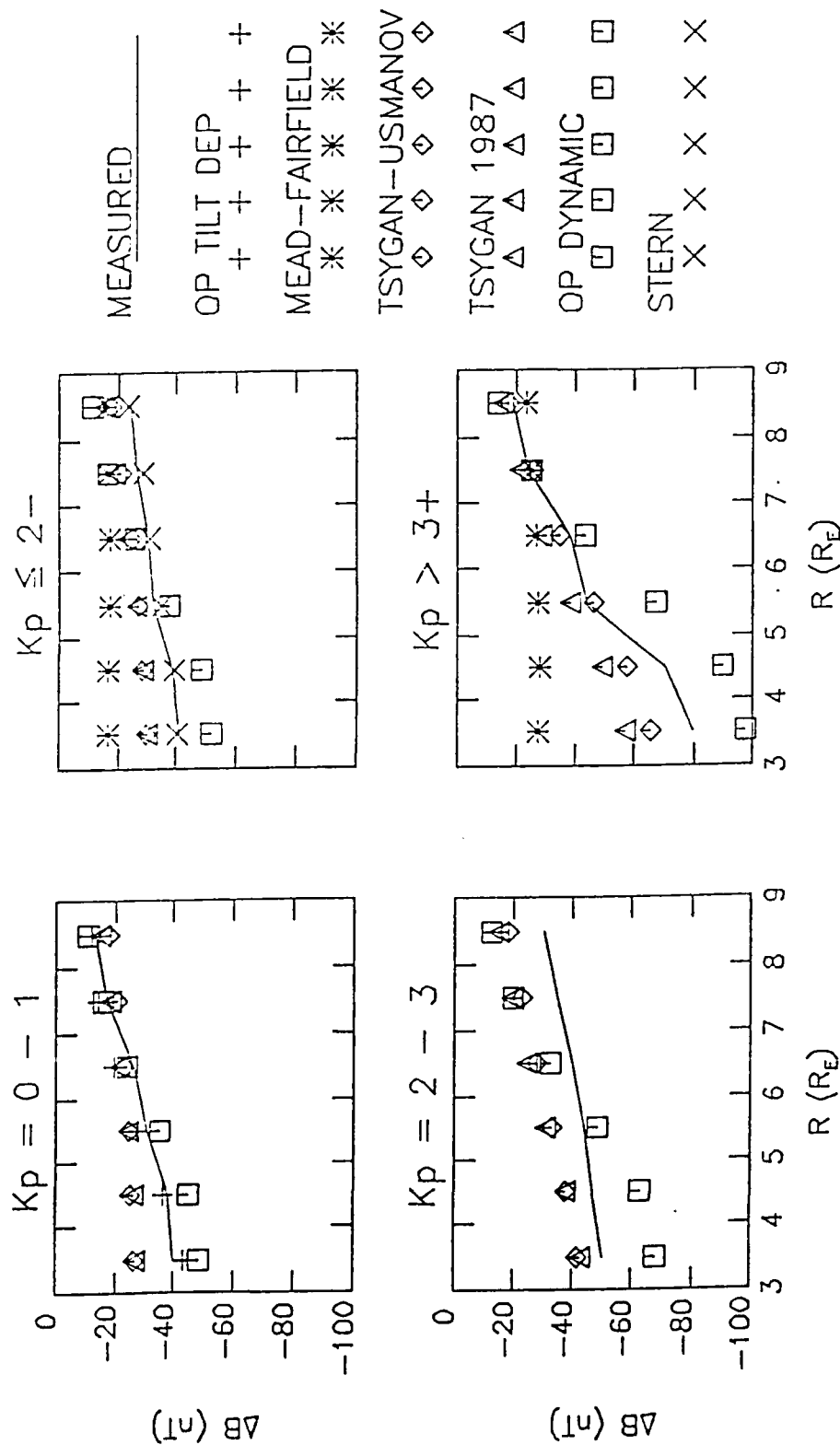Figure 16. Same as Figure 13, but for 21 April, 1979.

Figure 17. Averaged measured [*Fairfield, et al.,* 1987] and model midnight equatorial magnetic field depression. The $K_p = 0$-1 and 2-3 measurements are from OGO data, the $K_p \leq 2$ and $K_p \geq 3+$ measurements are from AMPTE data.

for the other two bins were determined by Fairfield, et. al. [1987] from the AMPTE/CCE data. According to the latter authors, some differences in the processing of the data may have led to differences in the high Kp results for the two satellites at the larger distances; however, the smaller distance values seem consistent.

For each model the quantity plotted is

$$\Delta B = |B_{dip} + B_{ext}| - |B_{dip}|$$

for zero dipole tilt. The Olson-Pfitzer tilt-dependent model is presumably appropriate to the K_p = 0-1 bin. For the Mead-Fairfield, Tsyganenko-Usmanov, and Tsyganenko 1987 short models, we chose bins as close to those of the data as the binning structure of the individual models permitted. Thus, the Mead-Fairfield model is specified for 4 bins. Of these, only two, $K_p < 2$ and $K_p \geq 3$ were sufficiently comparable to the data bins. For the Tsyganenko-Usmanov and Tsyganenko 1987 models, the results were obtained by weighted averaging of appropriately selected model bins; the number of observations in each such bin, given by the authors, determined the weighting factor for that bin. For example, the $K_p = 0$-1 bin for the Tsyganenko-Usmanov model was constructed from model calculations for the Kp = 0, 0+, 1-, and 1 bins used by the authors. The data sets used by the authors in the least squares fits for these bins contained, respectively, 634, 1553, 1784, and 1754 observations. Therefore, for the 0-1 bin:

$$\Delta B = (634 \ \Delta B_0 + 1553 \ \Delta B_{0+} + 1784 \ \Delta B_{1-} + 1754 \ \Delta B_1)/5725$$

For the Olson-Pfitzer model, the mean standoff distance and DST value for each K_p bin were determined from 1983 data on the NSSDC OMNI online data base. These are given in Table 4. In the Stern model, as for the Olson-Pfitzer tilt dependent model, only a single set of results is given.

Table 4. Average Values for the Olson-Pfitzer Dynamic Model

Kp	Standoff Distance	DST	No. of points
0-1	9.680	-1.1	440
0-2-	9.601	-2.3	819
2-3	9.091	-7.9	1098
≥ 3+	8.514	-28.0	1262

The Olson-Pfitzer tilt-dependent model agrees quite well with the measurements for the low K_p bin. This is not surprising, as this model is also derived from OGO data. The Mead-Fairfield, Tsyganenko-Usmanov, and Tsyganenko models all predict depressions smaller than the data at smaller distances. The K_p dependence in the Mead-Fairfield model is nearly constant with distance, while in the other two models the K_p dependence decreases with increasing distance, in apparent contrast with the data. The disagreement at small distances is probably due to the lack of equatorial data at these distances in the data sets used to derive these models. The Olson-Pfitzer dynamic model exhibits considerably greater depression than the data. Like the Tsyganenko-Usmanov and Tsyganenko model depressions, that for the Olson-Pfitzer dynamic model exhibits decreasing K_p dependence with increasing distance. The Stern model seems to fit the $K_p \leq 2$- measured depression, which is not too surprising, as Stern's dipole stretch model is based on data averaged over all geomagnetic activity levels.

36

6. SUMMARY AND CONCLUSIONS

Six models of the external magnetospheric field have been reviewed. The purpose of these models is to provide accurate and computationally efficient evaluation of the contribution to the magnetospheric magnetic field due to external sources, for use in analysis and interpretation of magnetospheric data. Five of these models were derived by fits of extensive data bases to analytical frameworks. Of these, the Mead-Fairfield model is the simplest computationally, with no explicit description of individual current systems contributing to the field. The Olson-Pfitzer tilt dependent was derived first as a fit of the data to wire models of three current systems: the ring currents, the magnetopause currents, and the cross-tail currents. Then the total numerical model was fit to sums of simple analytic functions. The resulting code, like that for the Mead-Fairfield model, therefore contains no explicit description of the individual current systems. The Tsyganenko-Usmanov, Tsyganenko, and Olson-Pfitzer dynamic models are composed of analytic expressions for the contributions of each of the three above-mentioned current systems. The Olson-Pfitzer data base is better rounded than those used for the other three, since it extends to smaller radial distances. The sixth model, Stern's parabolic magnetopause/stretched magnetosphere model, uses data to determine the stretched dipole representation of the tail field, but its magnetopause field is purely theoretical, and also very time-consuming to compute. None of the models explicitly represents a fourth current system, the field-aligned currents.

Of the six models, only the Olson-Pfitzer dynamic model contains no dipole tilt dependence. It is valid for zero tilt only. The Olson-Pfitzer tilt dependent model, unfortunately, is the only one that doesn't contain dynamic variations. The only dynamic variation presently in Stern's model is the magnetopause scaling with standoff distance. The Olson-Pfitzer dynamic model contains this plus the use of the DST index to derive the ring current strength. At present, the tail currents are tied to the magnetopause scaling, but this may not be realistic. The other three models are tied to the K_p index. They were each derived for individual K_p bins.

The properties of the models were examined in the 3-10 R_E range, that portion of the CRRES orbit where the external field is expected to be important. An external field typically modifies the L parameter beyond 4 R_E. The dependence of L on the dipole tilt is small along the dipole equator, but significant at higher latitudes.

For a magnetically quiet period, the magnetic field magnitudes derived from all the models agree closely with that derived from SCATHA magnetometer observations over that period. Upon closer review, it was found that the Olson-Pfitzer dynamic model tracks the data best, since its magnetopause model depends explicitly on the standoff distance. Stern's model, although its magnetopause model is also tied to the standoff distance, showed the poorest agreement with the data, possibly because its magnetopause model is purely theoretical, and its tail field, implied by the stretch model, is too large (and negative) on the night side and identically zero on the day side. During a substorm on the following day, none of the models predict the large drop in the field magnitude that is seen by the data, although several of the models show a very small decrease.

For zero tilt, the Stern and Olson-Pfitzer tilt-dependent model-calculated equatorial midnight field depressions are consistent with averaged AMPTE and OGO measurements as functions of distance. The Olson-Pfitzer dynamic model predicts larger depressions than observed, while the other dynamic models predict smaller depressions.

Although it is very difficult to select a single model which is optimal over all regions and levels of activity of the magnetosphere, at this point we recommend the Olson-Pfitzer dynamic model for use on CRRES. In this model the current systems are controlled by parameters directly affecting the dynamics of the magnetosphere: the solar wind speed and pressure, from which the noon magnetopause standoff distance can be determined, and the DST index, from which the ring current strength can be estimated. However a drawback at present is the scaling of the tail currents to the magnetopause standoff distance, rather than some other observable that would more directly relate to solar wind-tail coupling. The second reason for selecting the Olson-Pfitzer model is that its data base covers the inner region of CRRES's range better than the data bases used for the other models.

Principal drawbacks of the Olson-Pfitzer dynamic model are its lack of tilt dependence, its non-zero divergence, and the above-mentioned lack of a reliable tail parameter. In time, an improved model could be developed which includes tilt, and is rigorously divergence-free.

References

Bass, J. N., Gussenhoven, M. S., and Redus, R. H., "The Importance of Adiabatic Variations in Trapped Particle Distributions Observed by the SCATHA Satellite", GL-TR-89-0233, 1989.

Behannon, K. W., "Mapping of the Earth's Bow Shock and Magnetic Tail by Explorer 33", J. Geophys. Res., Vol. 73, Pp. 907-930, 1968.

Behannon, K. W., "Geometry of the Geomagnetic Tail", J. Geophys. Res., Vol. 75, P. 743, 1970.

Fairfield, D. H., "Average Magnetic Field Configuration of the Outer Magnetosphere", J. Geophys. Res., Vol. 73, Pp. 7329-7338, 1968.

Fairfield, D. H., "Bow Shock Associated Waves Observed in the Far Upstream Interplanetary Medium", J. Geophys. Res., Vol. 74, Pp. 3541-3553, 1969.

Fairfield, D. H., "Average and Unusual Locations of the Earth's Magnetopause and Bow Shock", J. Geophys. Res., Vol. 76, Pp. 6700-6716, 1971.

Fairfield, D. H., "Whistler Waves Upstream from Collisionless Shocks", J. Geophys. Res., Vol. 79, Pp. 1368-1378, 1974.

Fairfield, D. H., and Ness, N. F., "Configuration of the Geomagnetic Tail During Substorms", J. Geophys. Res., Vol. 75, Pp. 7032-7047, 1970.

Fairfield, D. H., and Ness, N. F., "IMP 5 Magnetic Field Measurements in the High-Latitude Outer Magnetosphere Near the Noon Meridian", J. Geophys. Res., Vol. 77, Pp. 611-623, 1972.

Fairfield, D. H., Acuna, M. H., Zanetti, L. J., and Potemra, T. A., "The Magnetic Field of the Equatorial Magnetotail: AMPTE/CCE Observations at R < 8.8 R_E", J. Geophys. Res., Vol. 92, No. A7, Pp. 7432-7442, 1987.

Hedgecock, P. C., and Thomas, B. T., HEOS Observations of the Configuration of the Magnetosphere", Geophys. J. R. Astr. Soc., Vol. 41, P. 391, 1975.

Jordan, C. E., and Bass, J. N., Evaluation of Magnetospheric Internal Magnetic Field Models and Existing Software, submitted for publication as GL Tech. Report, 1989.

McIlwain, C. E., "Coordinates for Mapping the Distribution of Magnetically Trapped Particles", J. Geophys. Res., Vol. 66, No. 11, Pp. 3681-3691, 1961.

Mead, G. D., "Deformation of the Geomagnetic Field by the Solar Wind", J. Geophys. Res., Vol. 69, Pp. 1181-1195, 1964.

Mead, G. D., and Fairfield, D. H., "A Quantitative Magnetospheric Model Derived from Spacecraft Magnetometer Data", J. Geophys. Res., Vol. 80, No. 4, Pp. 523-534, 1975.

Meng, C. I., and Mihalov, J. D., "Average Plasma Sheet Configuration at 60 Earth Radii", J. Geophys. Res., Vol. 77, P. 1739, 1972.

References (Cont'd)

Mihalov, J. D., Colburn, D. S., Currie, R. G., and Sonett, C. P., "Configuration and Reconnection of the Geomagnetic Tail", J. Geophys. Res., Vol. 73, P. 943, 1968.

Murayama, T., "Spatial Distribution of Energetic Electrons in the Geomagnetic Tail", J. Geophys. Res., Vol. 71, Pp. 5547-5557, 1966.

Olson, W. P., "The Shape of the Tilted Magnetopause", J. Geophys. Res., Vol. 74, No. 24, Pp. 5642-5651, 1969.

Olson, W. P., "A Model of the Distributed Magnetospheric Currents", J. Geophys. Res., Vol. 79, No. 25, Pp. 3731-3738, 1974.

Olson, W. P., and Pfitzer, K. A., "A Quantitative Model of the Magnetospheric Magnetic Field", J. Geophys. Res., Vol. 79, No. 25, Pp. 3739-3748, 1974.

Olson, W. P., and Pfitzer, K. A., Magnetospheric Magnetic Field Modeling, Annual Scientific Report, AFOSR Contract No. F44620-75-C-0033, McDonnell Douglas Astronautics Company, Huntington Beach, CA, 1977.

Olson, W. P., and Pfitzer, K. A., "A Dynamic Model of the Magnetospheric Magnetic and Electric Fields for July 29, 1977", J. Geophys. Res., Vol. 87, No. A8, Pp. 5493-5498, 1982.

Pfitzer, K. A., Olson, W. P., and Mogstad, T., "A Time Dependent, Source Driven Magnetospheric Magnetic Field Model" EOS, Vo. 69, No. 16, P. 426, 1988.

Pfitzer, K. A., Private Communication, 1989.

Press, W. H., Flannery, B. P., Teukolsky, S. A., and Vetterling, W. T., Numerical Recipes: The Art of Scientific Computing, Cambridge University Press, Cambridge/New York/New Rochelle/Melbourne/Sydney, 1986.

Radex, Inc., CRRES Data Processing Ephemeris Generating System System Product Development Specification, 1987.

Russell, C. T., "Geophysical Coordinate Transformations", Cosmic Electrodynamics, Vol. 2, Pp. 184-196, 1971.

Speiser, T. W., and Ness, N. F., "The Neutral Sheet in the Geomagnetic Tail: Its Motion, Equivalent Currents, and Field Line Connection Through It", J. Geophys. Res., Vol. 72, Pp. 131-141, 1967.

Stern, D. P., "Representation of Magnetic Fields in Space", Rev. Geophys. and Space Phys., Vol. 14, No. 2, Pp. 199-214, 1976.

Stern, D. P., "Parabolic Harmonics in Magnetospheric Modeling: The Main Dipole and the Ring Current", J. Geophys. Res., Vol. 90, No. A11, Pp. 10,851-10,863, 1985.

Stern, D. P., "Tail Modeling in a Stretched Magnetosphere 1. Methods and Transformations", J. Geophys. Res., Vol. 92, No. A5, Pp. 4437-4448, 1987.

References (Cont'd)

Sugiura, M., Ledley, B. G., Skillman, T. L., and Heppner, J. P., "Magnetic Field Distortions Observed by OGO 3 and 5", J. Geophys. Res., Vol. 67, P. 7552, 1971.

Sugiura, M., and Poros, D. J., "A Magnetospheric Field Model Incorporating the OGO 3 and 5 Magnetic Field Observations", Planet. Space Sci., Vol. 21, Pp. 1763-1773, 1973.

Tsyganenko, N. A., "Global Quantitative Models of the Geomagnetic Field in the Cislunar Magnetosphere for Different Disturbance Levels", Planet. Space Sci., Vol. 35, No. 11, Pp. 1347-1358, 1987.

Tsyganenko, N. A., and Usmanov, A. V., "Determination of the Magnetosphereic Current System Parameters and Development of Experimental Geomagnetic Field Models Based on Data from IMP and HEOS Satellites", Planet. Space Sci., Vol. 30, No. 10, Pp. 985-998, 1982.

Voigt, G-H, "A Three-Dimensional, Analytical Magnetospheric Model with Defined Magnetopause", J. Geophys., Vol. 38, Pp. 319-346, 1973.